LITHOS 470–471 (2024) 107525

Contents lists available at ScienceDirect

LITHOS

journal homepage: www.elsevier.com/locate/lithos

A Jurassic metamorphic-anatectic event in the Jiaodong Peninsula, eastern China: Zircon and titanite U-Pb ages of migmatites and their implications

Lishuang Liu [a,b,c,*], Matthew J. Kohn [d], Jinghui Guo [c]

[a] Joint International Research Laboratory of Catastrophe Simulation and Systemic Risk Governance, Beijing Normal University, Zhuhai 519087, China
[b] School of National Safety and Emergency Management, Beijing Normal University, Zhuhai 519087, China
[c] State Key Laboratory of Lithospheric Evolution, Institute of Geology and Geophysics, Chinese Academy of Sciences, Beijing 100029, China
[d] Department of Geosciences, Boise State University, Boise, ID 83725, USA

ARTICLE INFO

Keywords:
Migmatite
Anatectic zircon
Partial melting
Jurassic
Jiaodong Peninsula

ABSTRACT

Migmatite, generated from anatexis or partial melting, links metamorphism with magmatism and can be used to investigate the source of magmas. Zircon and titanite, as refractory minerals in migmatite, can illuminate both the conditions of partial melting and the sources of associated granites. Mesozoic granitoids in the Jiaodong Peninsula, eastern China, have been studied extensively for their origins as partial melts of the lower continental crust. However, Jurassic metamorphism and partial melting of their hypothesized parent rocks have rarely been reported and discussed. In this study, we investigated the morphology, interior structure, U-Pb geochronology, and trace element compositions of zircon and titanite from diverse migmatites in the Yantai-Rushan area of the Jiaodong Peninsula. For leucosomes, inherited metamorphic and magmatic (or anatectic) zircon cores yield Paleoproterozoic ages, indicating a North China affinity; in contrast, anatectic zircon domains with high rare earth element concentrations show Jurassic ages of 160–154 Ma. For mafic melanosomes, metamorphic zircon and titanite yield ages of 154–149 Ma and c. 150 Ma, respectively; in contrast, two inherited metamorphic zircons record Triassic ages, suggesting an affinity with the ultrahigh-pressure rocks in the Sulu orogen. For granites, the oldest age of anatectic zircons is 175 Ma. Altogether, these data demonstrate a long-lived (c. 25 Myr), Jurassic, metamorphic-anatectic event in the Jiaodong Peninsula. These new findings prove that three lithotectonic units—the Jiaobei terrane, Sulu orogen, and preexisting granites in the Jiaodong Peninsula—were all sources for protracted Jurassic partial melting. This study deepens our understanding of the links between metamorphism and magmatism in demonstrating the diverse rock types that simultaneously source granites.

1. Introduction

Partial melting is a vital link between metamorphism and magmatism (Brown, 1994) insofar as melts that form during metamorphic and orogenic processes may segregate and coalesce to form magma bodies. Thus, partial melting plays an important role in the formation of magmas and differentiation of Earth's crust (Labrousse et al., 2011; Wang et al., 2014; Xu et al., 2002). Prior to segregation, the parent rock typically differentiates into melanosomes and leucosomes (Brown et al., 1995). Melanosomes represent the remnants from the parent rocks after melt loss, while leucosomes crystallize from melt with minor residual minerals derived from their sources (Brown et al., 2016). Zircon, as a U-rich, refractory mineral that commonly survives metamorphism and melting, has very low rates of Pb diffusion (closure temperatures of c. 1000 °C; Cherniak and Watson, 2001). Titanite, a common accessory mineral in metamorphosed igneous rocks and calc-alkaline plutons, also often has high U content and has very low Pb diffusion rates (closure temperatures of c. 800 °C; Kohn, 2017). Thus, zircon and titanite U-Pb geochronology of migmatites can readily record the timing of peak metamorphism and partial melting as well as magmatism (Chen et al., 2015; Kohn, 2017; Xu et al., 2013; Xu and Zhang, 2017).

Large volumes of Mesozoic (Triassic, Jurassic, and Cretaceous) granitoids are widely distributed in the Jiaodong Peninsula, which spans the junction between the North China block and the Sulu orogen (Fig. 1; Guo et al., 2005; Hacker et al., 2006; Jiang et al., 2012; Zhao et al., 2017b). Among these granitoids, Triassic plutons were generated from

* Corresponding author at: Joint International Research Laboratory of Catastrophe Simulation and Systemic Risk Governance, Beijing Normal University, Zhuhai 519087, China.
E-mail address: liulishuang13@126.com (L. Liu).

https://doi.org/10.1016/j.lithos.2024.107525
Received 14 October 2023; Received in revised form 26 January 2024; Accepted 26 January 2024
Available online 1 February 2024

post-orogenic melting of refractory, re-enriched lithospheric mantle (Gao et al., 2023; Xu et al., 2016; Yang et al., 2005a). In contrast, Jurassic and Cretaceous granitoids are commonly interpreted to have been derived from the melting of thickened lower continental crusts during extension and thinning associated with Paleo-Pacific plate subduction (e.g., Wu et al., 2020 and references therein). Jurassic granites are the most important constituents of the Kunyushan and Linglong plutons in the Jiaodong Peninsula (Ma et al., 2013; Meng and Lin, 2021), which help define interpretations of the post-collisional evolution of the Sulu orogen. However, the present interpretation of the origin of the Jurassic granitoids is mainly based on geochemical data from the plutons, with little direct investigation of source rocks (Jiang et al., 2012; Li et al., 2019; Ma et al., 2013; Yang et al., 2012; Zhao et al., 2017a).

Direct evidence for Mesozoic melting of the mid- to lower crust is sparse in the Sulu orogen. Granitic leucosomes with Triassic (219–201 Ma) anatectic zircons discovered within amphibolites, paragneisses, and orthogneisses (Liu et al., 2010a, 2012) indicated a Triassic partial melting event. Evidence of melt crystallization after omphacite-breakdown in ultrahigh-pressure (UHP) eclogites further indicates partial melting during exhumation of the deeply subducted continental crust (Feng et al., 2021). However, this melt source (subducted crust) differs from previously inferred melt sources for Triassic plutons (enriched lithospheric mantle; Yang et al., 2005a). Late Jurassic (156–151 Ma) leucosomes with anatectic zircons have also been discovered within UHP rocks from the Sulu orogen (Liu et al., 2012), and could potentially have sourced Jurassic plutons (with a crustal source). In contrast, Late Jurassic metamorphism and partial melting of rocks with a North China affinity are virtually unknown; identification of a North China block source for any plutons would be important for tracing their origin(s) and genesis and for linking metamorphism and magmatism.

Here, we studied the detailed petrology, morphology, cathodoluminescence character, U-Pb geochronology, and trace element compositions of zircons and titanites from felsic and mafic migmatites and granites from the Yantai-Rushan area of the Jiaodong Peninsula, eastern China. This study not only provides key information for Jurassic metamorphic-anatexis of Precambrian rocks but also further constrains the multiple origins of Jurassic granites.

2. Geological background and sampling

The Jiaodong Peninsula, located in eastern China, is divided by the Yantai-Qingdao-Wulian fault belt into the Jiaobei terrane to the west and the northern Sulu UHP orogen to the east (Fig. 1). The Jiaobei terrane belongs to the North China block and contains Archean-Paleoproterozoic rocks that experienced Paleoproterozoic granulite-facies metamorphism and partial melting (e.g., Liu et al., 2014a, 2017). The northern Sulu orogen represents the northeastern sector of the Sulu-Dabie orogen and consists of Neoproterozoic rocks of the South China block, overprinted by Triassic UHP metamorphism (Liu and Liou, 2011). Thus, protolith and metamorphic ages are expected to differ markedly between the two main lithotectonic units: the Jiaobei terrane (North China block) should exhibit Archean and Paleoproterozoic ages whereas the Sulu orogen (South China block) should exhibit Neoproterozoic and Triassic ages.

A striking feature of the Jiaodong Peninsula is the widespread Mesozoic granitoids that include Late Triassic alkaline and Late Jurassic to Early Cretaceous calc-alkaline rocks (Fig. 1b), all intruded into Precambrian basement (e.g., Guo et al., 2005; Hacker et al., 2006). Petrological and geochemical studies suggest that the plutons are products of partial melting of the exhumed or thickened lower continental crust or lithospheric mantle, related to the post-collisional magmatism between the North and South China blocks (Jiang et al., 2012; Ma et al., 2013; Xu and Zhang, 2017). In principle, partial melts from either the Jiaobei terrane or Sulu orogen could have sourced the granitoids, but direct evidence for anatexis is scarce (Feng et al., 2021; Liu et al., 2012).

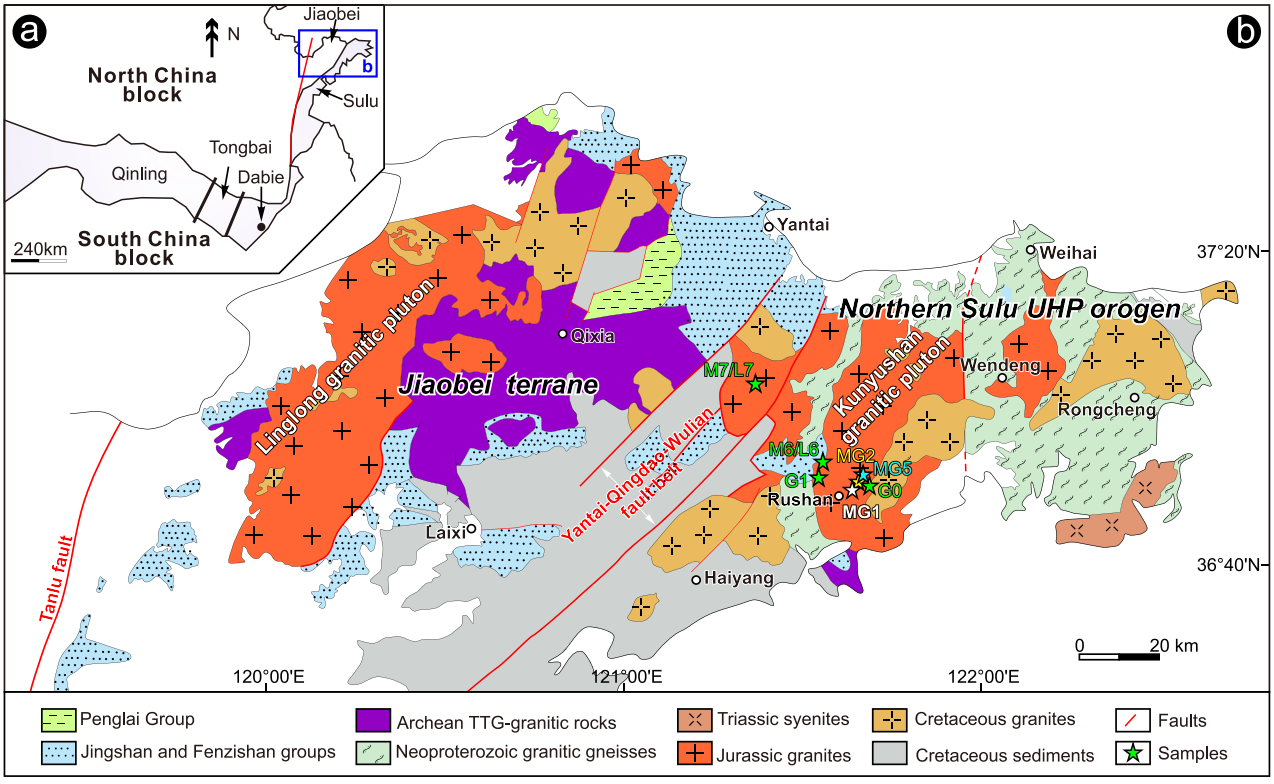

Fig. 1. Geological map of Jiaodong Peninsula, eastern China. The Jiaobei terrane, in the west, is a part of a Paleoproterozoic orogen in the North China block; the northern Sulu ultrahigh-pressure (UHP) orogen, in the east, represents the northeastern sector of the Triassic Dabie-Sulu orogen. The Yantai-Qingdao-Wulian fault belt separates the two terranes.

In this study, we focus on felsic and mafic migmatite, garnet amphibolite, and granite samples from the Yantai-Rushan area of the eastern Jiaodong Peninsula. The exposures of most samples are blocks of varying size, except that the felsic migmatites outcrop in layers (Fig. 2). Leucosomes from both the felsic and mafic migmatites occur commonly as veins in melanosomes (Fig. 2a, e), but melanosomes also occur as residues in pegmatitic leucosomes (Fig. 2b). We collected both melanosome and leucosome samples from felsic migmatites but only melanosome from mafic migmatite (Fig. 2a, b, e). The felsic melanosomes mainly contain plagioclase, K-feldspar, and quartz with diverse calcic and mafic minerals (such as epidote and biotite) (Fig. 2c), while the leucosomes consist of plagioclase, K-feldspar, and quartz with minor mafic minerals (Fig. 2d). The mafic melanosome sample MG2 and garnet amphibolite samples MG1 and MG5 from Rushan are composed of amphibole, plagioclase, and quartz with clinopyroxene or garnet (Fig. 2e–j). Former silicate melt was observed between amphibole grains as fine-grained aggregates (Fig. 2k). Granite samples G2 and G1 consist of plagioclase, K-feldspar, and quartz with minor biotite or garnet (Fig. 2l–o), similar mineralogically to the leucosomes in the migmatites.

3. Analytical methods

Zircon cathodoluminescence (CL) and titanite backscattered electron (BSE) images were collected and combined with transmitted- and reflected-light photomicrographs to reveal zircon and titanite internal structures. Zircon grains of samples M7, L7, M6, L6, MG1, and G1 and titanite grains of sample MG5 were analyzed by LA-ICP-MS for their U-Pb and trace element compositions, at Beijing Createch Testing Technology Co. Ltd. and Beijing Quick-Thermo Science and Technology Co. Ltd., respectively. U-Pb dating of zircon grains from mafic migmatite sample MG2 was performed on a SHRIMP II instrument at the Beijing SHRIMP Center, Institute of Geology, Chinese Academy of Geological Sciences (CAGS). Whole-rock major and trace element compositions were measured by X-ray fluorescence (XRF; PW4400) on fused glass beads and ICP-MS (PE300D), respectively, at the National Research Center of Geoanalysis, CAGS. Appendix A provides further detailed descriptions of analytical methods.

4. Results

The morphologies, CL-characteristics, U-Pb data, and trace element compositions of zircons and titanites from different samples are shown in Figs. 3–7 and/or listed in Supplementary Tables S1–S4. Whole-rock major and trace element compositions of migmatites and granite are reported in Fig. 8 and Supplementary Table S5.

4.1. Zircon U-Pb ages and rare earth element (REE) compositions of felsic migmatites

Zircon crystals from melanosome M7 and leucosome L7 are from directly adjacent samples, but have quite different CL characteristics (Fig. 3a, b). Zircon crystals from M7 are rounded and were subdivided into two groups. The first group (Group 1) has high CL intensity (Fig. 3a), low U contents (34–151 ppm) and high Th/U values (0.80–5.17), with a relatively tight age distribution and younger $^{207}Pb/^{206}Pb$ ages (1933–1714 Ma with a weighted mean age (WMA) of 1849 ± 17 Ma, MSWD = 1.3) (Fig. 3c; Table S1). The second group (Group 2) has low CL intensity (Fig. 3a), high U contents (139–1968 ppm) and low Th/U values (0.02–1.10) and has more scattered and generally older $^{207}Pb/^{206}Pb$ ages of 2144–1783 Ma (Table S1). Group 2 zircons can be further divided into two categories based on their ages (Fig. 3c; Table S1): the first category (Group 2a) comprises zircon grains with significantly older $^{207}Pb/^{206}Pb$ ages ranging from 2144 to 2005 Ma, with a WMA of 2040 ± 28 Ma (MSWD = 1.9); the second category (Group 2b) consists of zircon grains with younger $^{207}Pb/^{206}Pb$ ages ranging from 1940 to 1783 Ma, with a WMA of 1890 ± 12 Ma (MSWD = 1.5). Almost all the zircon grains from groups 1, 2a, and 2b show negative Eu anomalies (Eu/Eu* < 1.0) in Chondrite-normalized REE diagrams (Fig. 3d; Table S2). However, zircon grains of Group 2a exhibit the highest heavy rare earth element (HREE) concentrations and the most pronounced negative Eu anomalies, while those of Group 2b display the lowest HREE concentrations and moderate Eu anomalies. In contrast, zircon grains of Group 1 have moderate HREE anomalies and the highest Eu/Eu* values (Fig. 3d; Table S2).

Zircon crystals from leucosome L7 are euhedral and prismatic with length-width ratios of 2.5:1 to 2:1. Most zircon grains have high-luminescence cores and low-luminescence rims (Fig. 3b). Thirteen cores record $^{207}Pb/^{206}Pb$ ages of 2103–1847 Ma, overlapping ages for M7 group 2 zircons, while the other twelve cores yield $^{206}Pb/^{238}U$ ages of 165–149 Ma. Regressing core data alone, the lower intercept age (154 ± 21 Ma; MSWD = 4.0) is statistically indistinguishable from ages of the twenty-five rims (164–139 Ma with a WMA of 155 ± 2 Ma, MSWD = 1.3) (Fig. 3e; Table S1). Zircon rims show higher U and HREE contents than cores, and both show negative Eu anomalies (Fig. 3f; Tables S1, S2).

Zircon crystals from melanosome M6 and associated leucosome L6 are subhedral with length-width ratios of 3:2 to 2:1 (Fig. 4a, b). Zircon crystals from M6 are dark with slight zoning in CL images (Fig. 4a), and have relatively high U contents of 1243–4304 ppm and low Th/U values of 0.05–0.16 (Table S1). Forty-nine analyses yield a range of $^{207}Pb/^{206}Pb$ ages of 1933–1809 Ma with a well-defined WMA of 1870 ± 7 Ma (MSWD = 0.91; Fig. 4c). These analyses show high total rare earth element (ΣREE) contents (292–1030 ppm) with high HREE contents, low light REE (LREE) contents, and pronounced negative Eu anomalies (Eu/Eu* up to 0.66) (Fig. 4d; Table S2).

In contrast, zircon grains from L6 are smaller and have high-luminescence cores and low-luminescence rims (Fig. 4b). Zircon cores yield two groups of $^{207}Pb/^{206}Pb$ ages of 2116–1791 Ma (n = 7) and 780–305 Ma (n = 22; Fig. 4e; Table S1). Fourteen analyses of zircon rims show high U contents and low Th/U values and yield a $^{206}Pb/^{238}U$ age range of 166–153 Ma with a weighted mean of 160 ± 4 Ma (MSWD = 2.0; Fig. 4f). Both zircon cores and rims have widely varying REE contents (70–3409 ppm) with pronounced negative Eu anomalies (Eu/Eu* = 0.05–0.59 for the cores and Eu/Eu* = 0.27–0.97 for most rims; Fig. 4g, h; Table S2).

4.2. Zircon U-Pb ages and REE compositions of mafic melanosome and garnet amphibolite

Zircon grains of mafic migmatite MG2 and garnet amphibolite MG1 are small (< 80 μm; Fig. 5a, b). Some grains show patchy luminescence while others show homogenous gray-luminescence. Seventeen of eighteen analyses of the gray domains from MG2 that have low Th/U values (0–0.08) give $^{206}Pb/^{238}U$ ages of 159.1–145.4 Ma with a WMA of 153.8 ± 1.9 Ma (MSWD = 1.3) (Fig. 5c; Table S1). These domains have high ΣREE and HREE contents with negative Eu anomalies (Eu/Eu* = 0.38–0.89) (Fig. 5d; Table S2); these geochemical observations (especially their low Th/U values) indicate they are metamorphic in origin. Eight of ten analyses from MG1 have low Th/U values (0–0.06) and yield $^{206}Pb/^{238}U$ ages of 153–145 Ma with a WMA of 149 ± 4 Ma (MSWD = 0.4); the other ages are Triassic and range from 234 to 221 Ma (Fig. 5e; Table S1). Jurassic metamorphic zircons have markedly higher HREE contents and steeper HREE patterns than the Triassic zircons (Fig. 5f; Table S2).

4.3. Zircon U-Pb ages and REE compositions of granites

Zircon grains from granite G0 and G1 are euhedral and elongated with length-width ratios are 4:1 to 2:1 (Fig. 6a, b). Most grains have high-luminescence cores and low-luminescence rims. Twelve analyses of G0 define an isochron with an upper intercept of 753 ± 41 Ma and a lower intercept of 159.2 ± 4.7 Ma (Fig. 6c). A subset of nine concordant analyses yields an age range of 165.0–156.4 Ma with a WMA of 161.0 ±

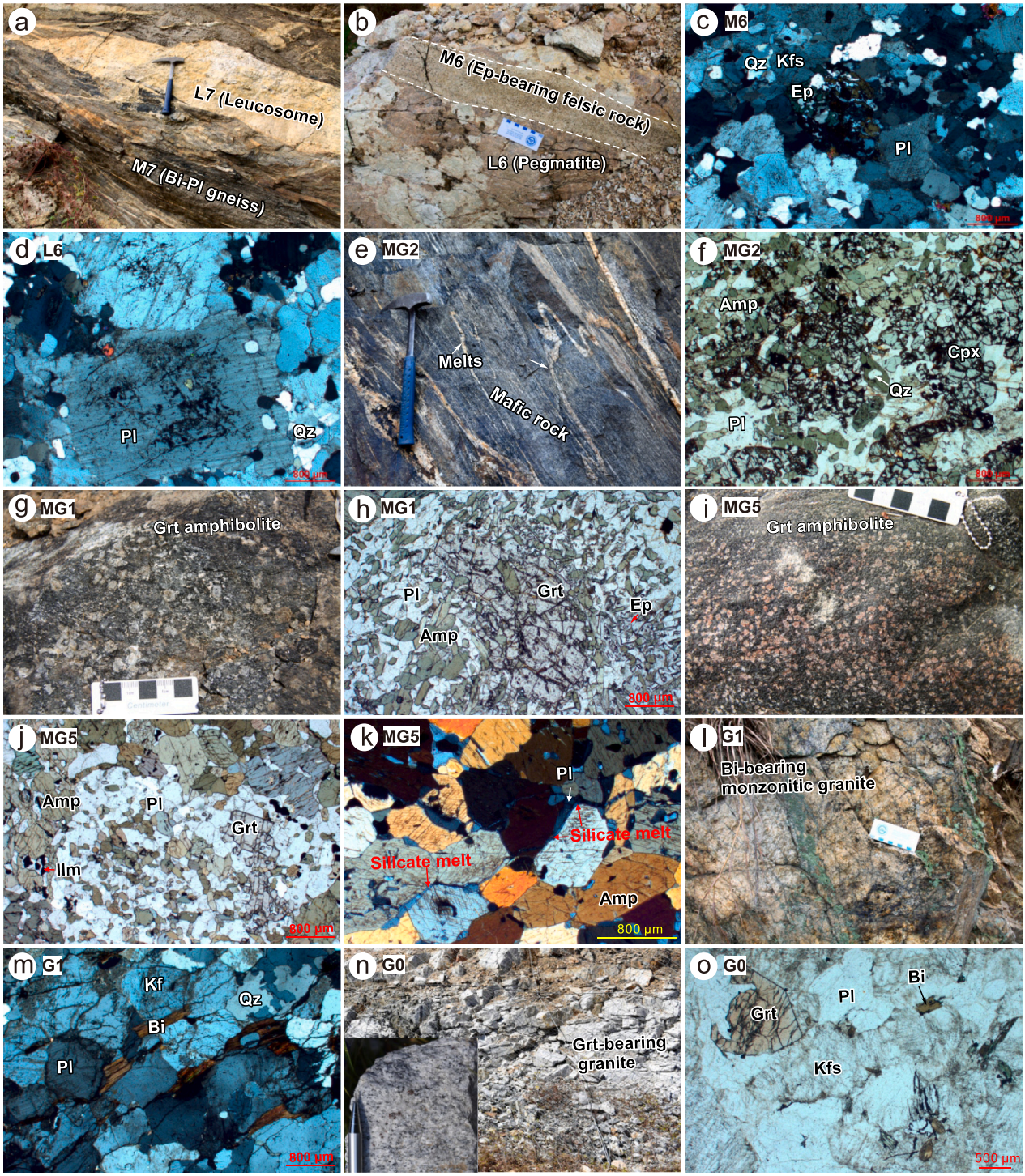

Fig. 2. Field photographs and photomicrographs of migmatites and granites. (a) Biotite-plagioclase gneiss occurs as melanosome (M7) with coexisting leucosome (L7). (b) Epidote-bearing felsic rock occurs as relict "melanosome" (M6) in pegmatitic leucosome (L6). (c) Melanosome sample M6 is composed of plagioclase, K-feldspar, quartz, and epidote (under cross-polarized light). (d) Leucosome sample L6 is composed of coarse-grained plagioclase, K-feldspar, and fine-grained quartz (under cross-polarized light). (e) Mafic migmatite MG2 consists of clinopyroxene-bearing amphibolite (melanosome) with fine felsic veins (which probably represent melts). (f) Melanosome of MG2 mainly consists of amphibole, plagioclase, quartz, and clinopyroxene (under plane-polarized light). (g) Outcrop of garnet amphibolite (MG1) shows a "white-eye socket" texture in which garnets are surrounded by leucocratic materials. (h) Symplectites of amphibole + plagioclase surround relict garnet in MG1. (i, j) Outcrop and photomicrograph of garnet amphibolite MG5 show similar mineral assemblage and "white-eye socket" texture with MG1. (k) Silicate melt occurs as veinlet between amphibole grains. (l, m) Outcrop and photomicrograph of biotite-bearing monzonitic granite (G1). (n, o) Outcrop and photomicrograph of garnet-bearing granite (G0). Abbreviations: Bi, biotite; Grt, garnet; Ep, epidote; Qz, quartz; Kfs, K-feldspar; Pl, plagioclase; Amp, amphibole; Cpx, clinopyroxene; Ilm, ilmenite.

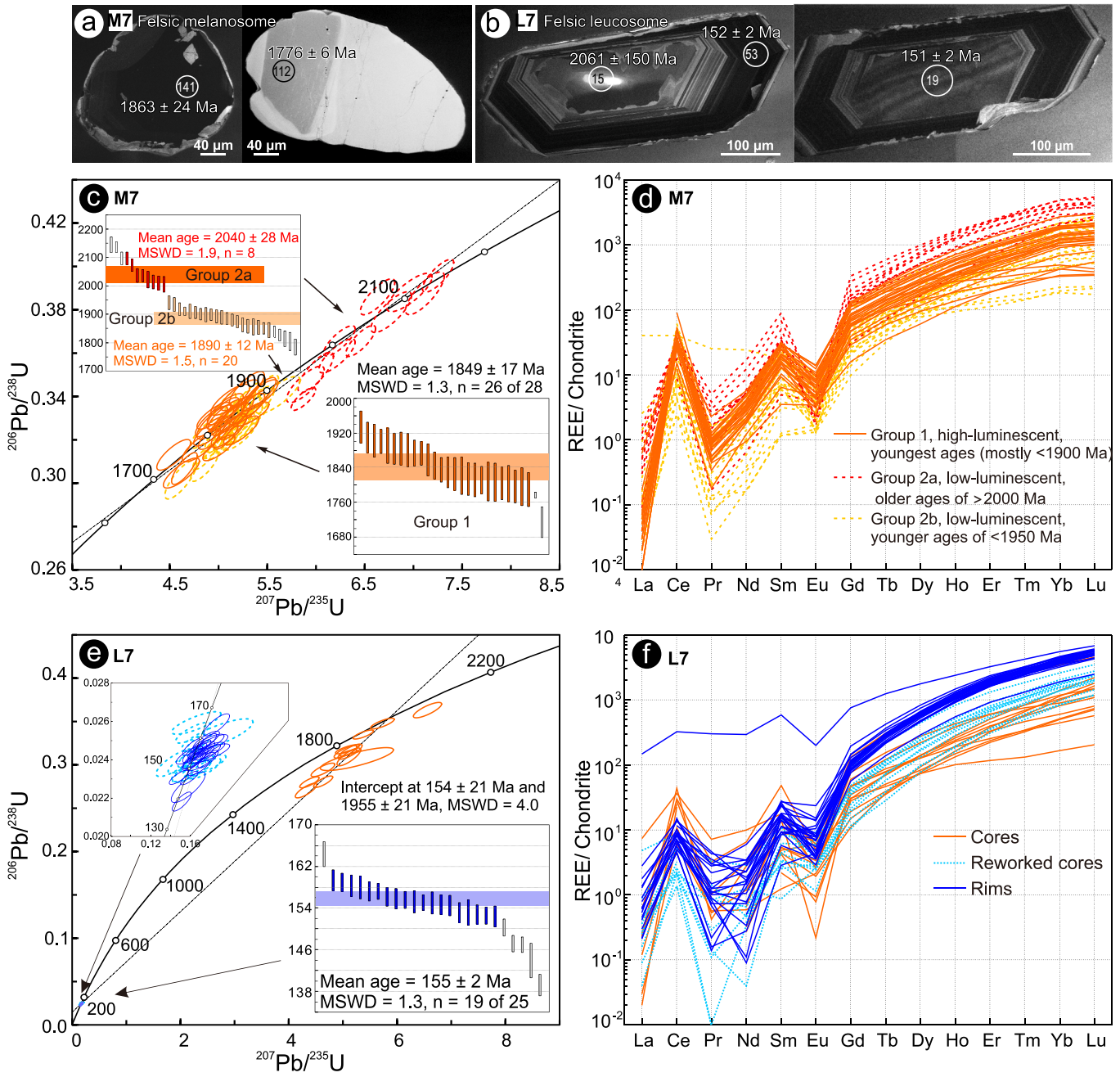

Fig. 3. Cathodoluminescence images and U-Pb concordia diagrams of zircons from melanosome sample M7 and leucosome sample L7. (a) Zircons from M7 are anhedral and both low- and high-luminescent. (b) Zircons from L7 are euhedral and prismatic with high-luminescence cores and low-luminescence rims. (c, d) U-Pb concordia diagram and corresponding rare earth element patterns of zircons from M7. (e, f) U-Pb concordia diagram and corresponding rare earth element patterns of zircons from L7.

2.2 Ma (Fig. 6d), within error of the lower intercept age.

Thirty analyses for the zircon cores in G1 give $^{206}Pb/^{238}U$ ages of 183–167 Ma with a WMA of 175 ± 2 Ma (MSWD = 1.6) (Fig. 6e; Table S1). Twenty-four and four analyses for the rims yield $^{206}Pb/^{238}U$ ages of 199–169 Ma and 159–147 Ma, respectively. The rims have much higher U contents (718–3767 ppm) and lower Th/U values (0.01–0.21) than the cores (U = 46–363 ppm, Th/U = 0.25–0.75). The zircon cores and rims have similar ΣREE contents and negative Eu anomalies, except that LREE contents of the rims vary more widely (Fig. 6f; Table S2).

4.4. Titanite U-Pb ages and REE compositions of garnet amphibolite

Titanite grains of garnet amphibolite MG5 are anhedral with diameters around 150–200 μm (Fig. 7a, b). Most grains are colorless to light yellow and transparent with sparse inclusions. BSE image shows that most titanite grains are homogeneous whereas others have slight irregular zoning. Twenty-three analyses of homogeneous domains yield a lower intercept age of 150 ± 16 Ma (MSWD = 1.7) as shown in a Tera-Wasserburg inverse concordia diagram (Fig. 7c; Table S3). These domains exhibit high HREE contents (41–554 ppm) with LREE patterns (La_N/Gd_N = 0–1.24) and variable ΣLREE contents (10–1109 ppm; Fig. 7d; Table S4). Overall, the Zr contents in the analyzed titanite grains are moderate, spanning between 38 and 206 ppm, corresponding to temperatures of c. 650–750 °C (assuming P = 8 kbar) based on Zr-in-titanite thermometry (Hayden et al., 2008).

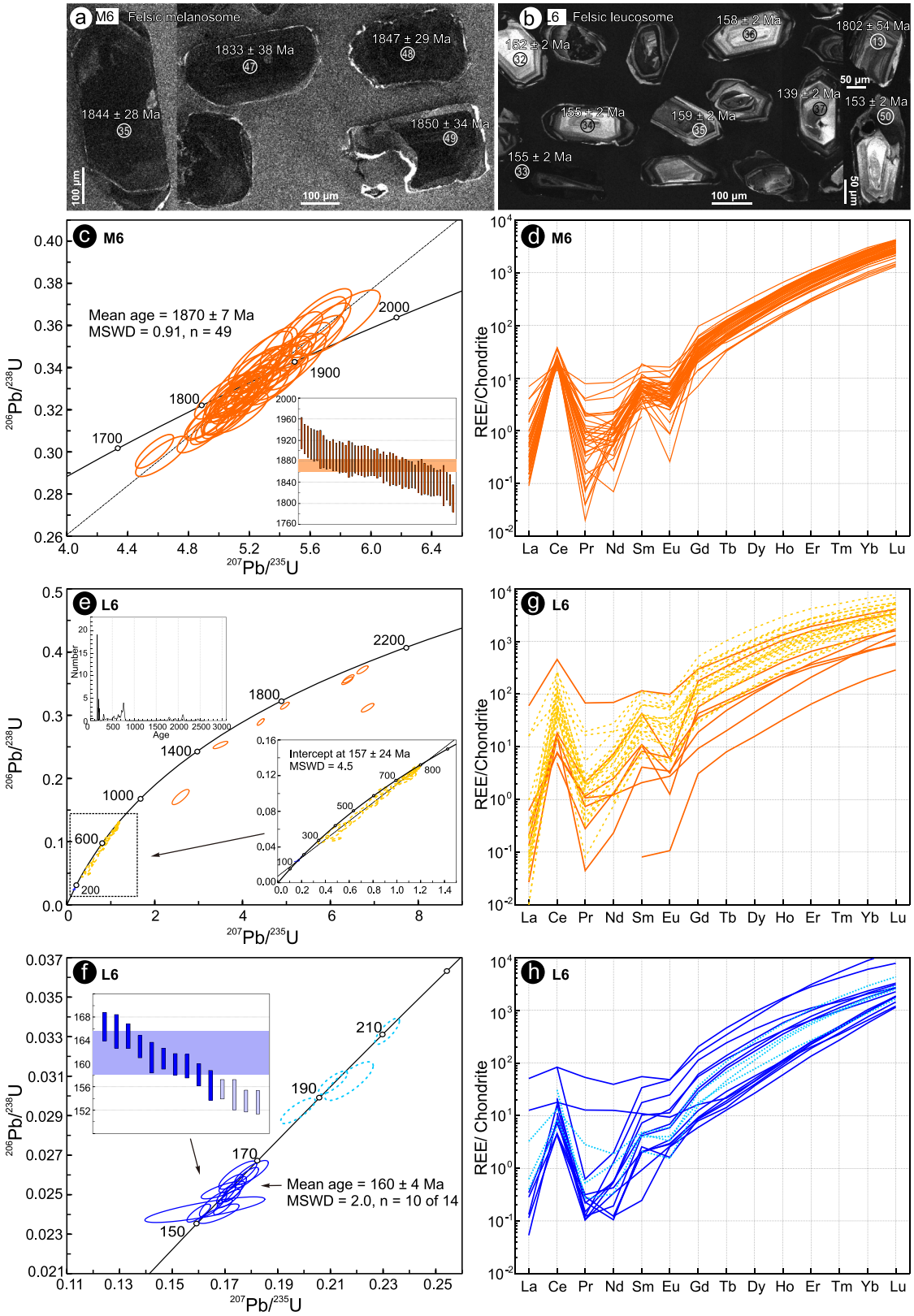

Fig. 4. Cathodoluminescence images and U-Pb concordia diagrams of zircons from melanosome sample M6 and leucosome sample L6. (a) Zircons from M6 are subhedral with low luminescence. (b) Zircons from L6 are euhedral and prismatic with high-luminescence cores and low-luminescence rims. (c, d) U-Pb concordia diagram and corresponding rare earth element patterns of zircons from M6. (e–h) U-Pb concordia diagrams and corresponding rare earth element patterns of zircons from L6.

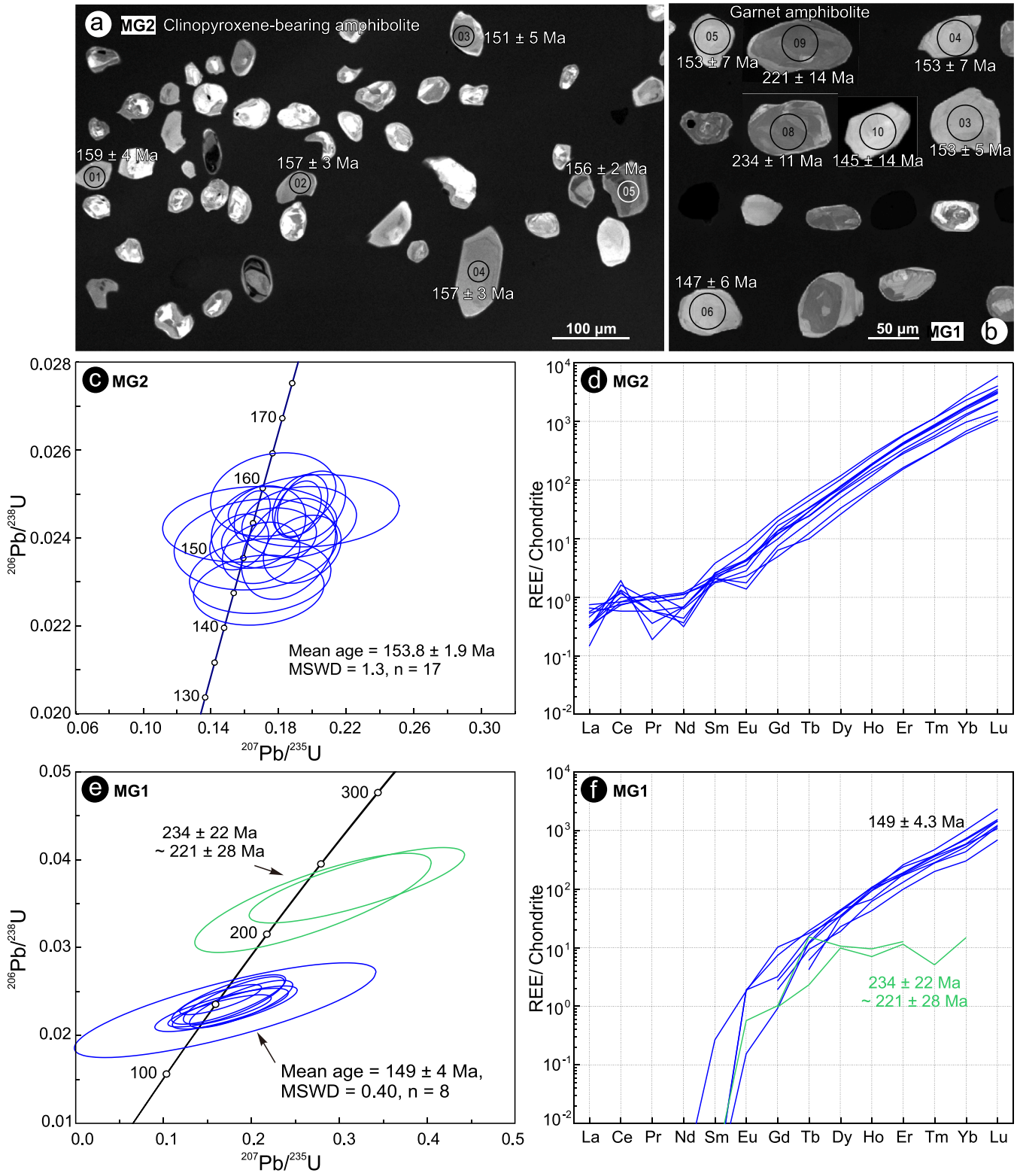

Fig. 5. Cathodoluminescence images and U-Pb concordia diagrams of zircons from the mafic melanosome samples MG2 and MG1. (a, b) Zircons are anhedral, and some have patchy luminescence whereas others have homogenous gray-luminescence. (c, d) U-Pb concordia diagram and corresponding rare earth element patterns of zircons from MG2. (e, f) U-Pb concordia diagram and corresponding rare earth element patterns of zircons from MG1.

4.5. Whole-rock geochemistry of migmatites and granite

Leucosome samples L7 and L6 and granite sample G1 exhibit similar major and trace element compositions. They all display high SiO_2 (72.27–73.99 wt%) and total alkali ($Na_2O + K_2O$) (4.91–9.17 wt%) contents, along with low MgO (0.11–0.83 wt%), CaO (0.75–2.24 wt%), and TiO_2 (0.09–0.82 wt%) contents (Table S5; Fig. 8a). The Al_2O_3, Fe_2O_3, and FeO contents range between 12.28 and 15.05 wt%, 1.01 and 2.09 wt%, and < 0.1 and 2.78 wt%, respectively. Trace element compositions of the leucosomes and granite exhibit minor differences but are

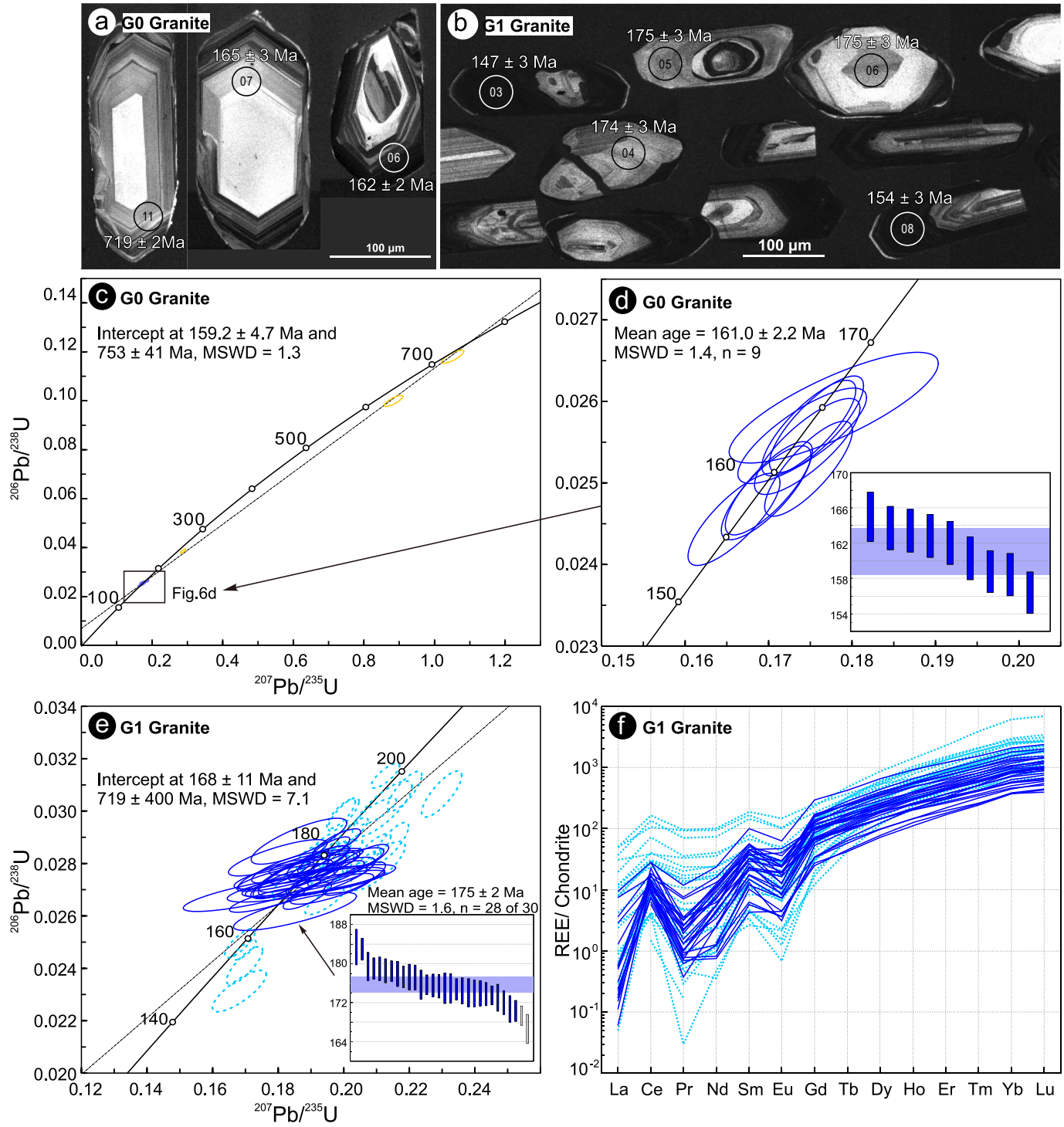

Fig. 6. Cathodoluminescence images and U-Pb concordia diagrams of zircons from granite samples G0 and G1. (a, b) Zircons from the two samples are elongated and euhedral with length-width ratios of 4:1 to 2:1. (c, d) U-Pb concordia diagrams of zircons from G0. (e, f) U-Pb concordia diagram and corresponding rare earth element patterns of zircons from G1.

largely comparable. For instance, the LREE contents are higher than the HREE contents, resulting in consistent REE patterns in a chondrite-normalized diagram (Fig. 8b). Large-ion lithophile elements (LILEs, such as Rb, Sr, and Ba) are enriched whereas high-field strength elements (HFSEs, such as Nb, Ta, Zr, and Hf) are depleted (Table S5). Relatively high Sr and low Y contents yield high Sr/Y values (Fig. 8c), indicating an affinity with adakite. In contrast, melanosome sample M7 has lower concentrations of HREE and displays a right-dipping REE pattern in a chondrite-normalized diagram, without any Eu anomaly (Fig. 8b).

5. Discussion

5.1. Protoliths of migmatite in the Jiaodong Peninsula

Migmatites in the Jiaodong Peninsula have been interpreted to contribute to formation of granitic plutons (Faure et al., 2003; Liu et al., 2012; Liu et al., 2014a; Zhao et al., 2017b). If so, unique metamorphic

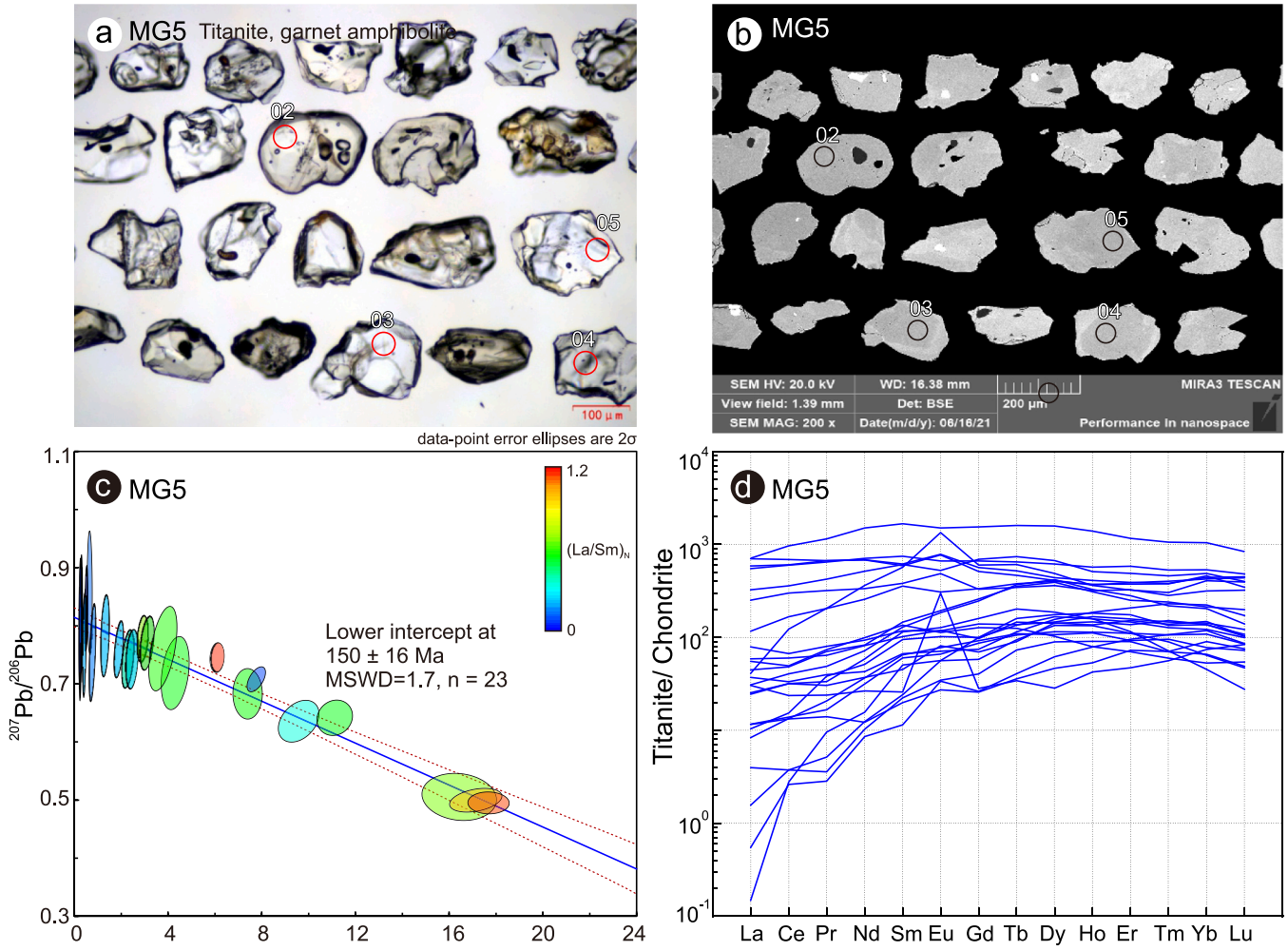

Fig. 7. Photomicrographs and U-Pb Tera-Wasserburg inverse concordia diagram of titanite from garnet amphibolite sample MG5. (a, b) Transmitted light and backscatter electron images of titanite grains that are colorless-light yellow, transparent, and irregularly shaped with some inclusions. (c, d) U-Pb Tera-Wasserburg inverse concordia diagram and corresponding rare earth element patterns of titanites. (For interpretation of the references to colour in this figure legend, the reader is referred to the web version of this article.)

characteristics should allow sources to be identified. As the southeastern part of the North China block, the Jiaobei terrane, experienced Paleoproterozoic medium- to high-pressure granulite-facies metamorphism along a clockwise *P–T* path (e.g., Liu et al., 2017). Paleoproterozoic partial melting has been identified from granitic leucosomes within granulite, amphibolite, and TTG gneisses (Li et al., 2017; Liu et al., 2019; Zou et al., 2018). Medium-P (5–8 kbar) partial melting at 1900–1850 Ma generally post-dated high-P (12.8–14.4 kbar) granulite-facies metamorphism at 1950–1900 Ma (Fig. 9a; Zhou et al., 2008; Tam et al., 2011; Liu et al., 2013, 2017; Li et al., 2017; Zhao et al., 2015; Zou et al., 2018, 2021) during exhumation of the Jiaobei terrane (Liu et al., 2019). Sparse, late Paleoproterozoic (c. 1800 Ma), post-orogenic granitoids that probably derived from partial melting of the thickened continental crust are sporadically exposed in the Jiaobei terrane (Liu et al., 2014b; Fig. 9a). Thus, Paleoproterozoic (metamorphic or anatectic) ages of 1950–1800 Ma, if present as relict grains, would indicate a Jiaobei source.

In contrast to the ancient origins of Jiaobei rocks, granitic gneisses, metasedimentary rocks, and eclogites from the Sulu orogen derived from much younger Neoproterozoic protoliths (c. 730 to 820 Ma; e.g., Guo et al., 2005; Hacker et al., 2006) that experienced Early-Middle Triassic (240–225 Ma) UHP eclogite-facies metamorphism, Late Triassic (220–205 Ma) retrograde amphibolite-facies metamorphism (Liu et al., 2010a, 2012; Liu and Liou, 2011), and subsequent partial melting at 219–200 Ma (Fig. 9b; Liu et al., 2010a, 2012; Xu et al., 2013; Feng et al., 2021). This partial melting has been ascribed to the exhumation of deeply subducted continental crust (e.g., Chen et al., 2013; Feng et al., 2021; Zhou et al., 2019) and interpreted to source post-orogenic magmatism during the Late Triassic (Yang et al., 2005a). Thus, Neoproterozoic or Triassic ages, if present as relict grains, would indicate a Sulu orogen source.

Melanosomes M7 and M6 as well as leucosomes L7 and L6 preserve abundant inherited Paleoproterozoic zircon (Figs. 3, 4, 8). For M7, zircon grains of Group 1 exhibit homogeneous gray-white CL characteristics (Fig. 3a), which is consistent with a metamorphic origin. Although their high Th/U values (0.80–5.17; Table S1) are not typical of metamorphic zircon, the U-Pb ages of c. 1849 Ma (Fig. 3c) correspond to the post-peak metamorphic stages of the Jiaobei terrane (Fig. 9a). Zircon grains of Group 2 display low CL intensity and relatively low Th/U values of 0.02–1.10, yielding two distinct age groups around 2040 Ma and 1890 Ma. The age of c. 1890 Ma, with Th/U values ranging from 0.02 to 1.10, aligns closely with the peak metamorphic age of the Jiaobei terrane. Conversely, the age of c. 2040 Ma, with Th/U values ranging from 0.18 to 0.09, is significantly older than the Paleoproterozoic metamorphic age of the Jiaobei terrane. According to a recent compilation of zircon compositions, metamorphic zircon can exhibit Th/U < 0.1 to >10, while igneous zircon rarely has Th/U < 0.1 (Yakymchuk et al., 2018). Together with variations in HREE contents and Eu/Eu*

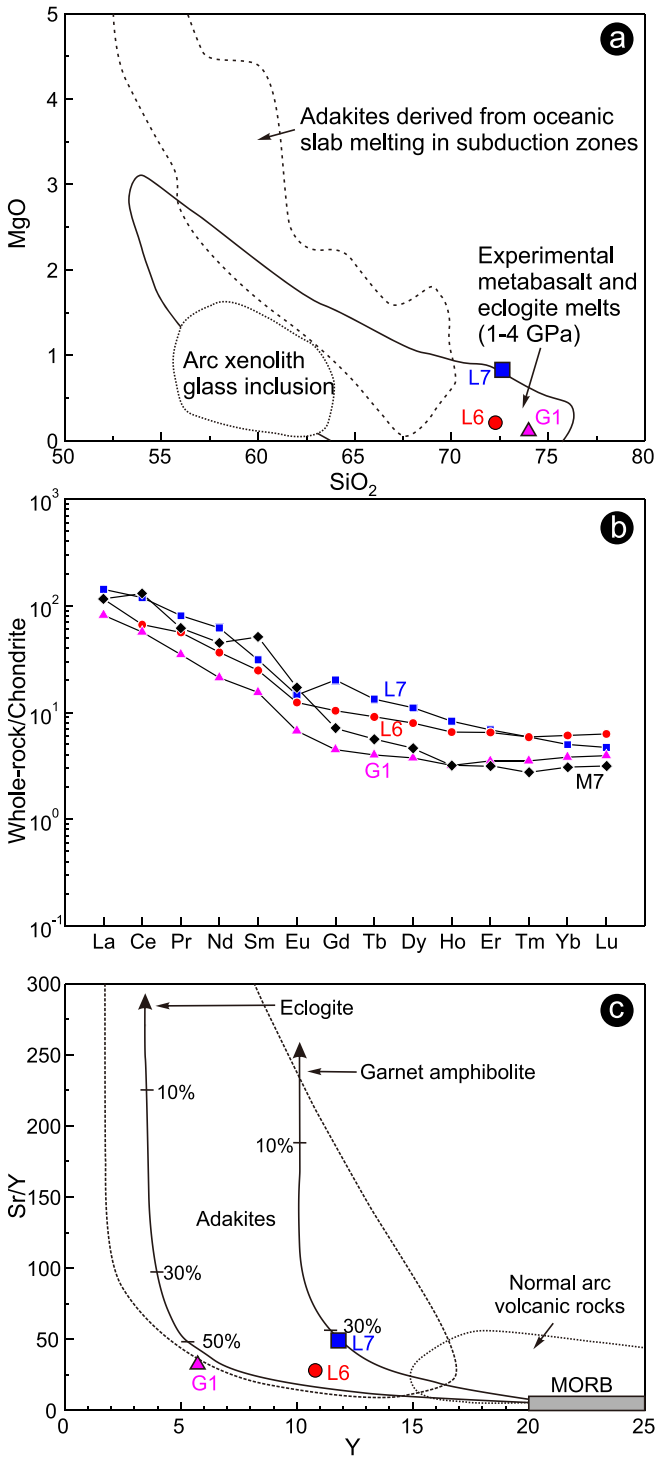

Fig. 8. Geochemical data of the migmatite and granite samples. (a) MgO versus SiO_2 diagram for leucosome and granite discriminating nature of rocks and melt sources (after Defant and Drummond,1990; Rapp et al., 1999); (b) Chondrite-normalized REE patterns of melanosome M7, leucosome L7 and L6, and granite G1; (c) Sr/Y versus Y diagram for leucosomes and granite discriminating adakites and normal volcanic rocks (after Defant and Drummond, 1990).

anomalies (Fig. 3d; Table S1), the zircon ages promote the following interpretations for the origins of each group: Group 2a zircon is likely inherited from protoliths prior to metamorphism, Group 2b zircon recrystallized in the presence of garnet during metamorphism, and Group 1 zircon formed during decompression and late-stage metamorphic overprinting. For M6 zircons, inherited cores show low luminescence with weak oscillatory zoning (Fig. 4a) and high U contents (1243–4304 ppm) with low Th/U values (0.05–0.16) (Table S1), indicating an anatectic origin. The U-Pb age of c. 1870 Ma (Fig. 4c) coincides with the timing of partial melting in the Jiaobei terrane (Fig. 9a). For leucosomes L6 and L7, inherited Paleoproterozoic zircon cores (Figs. 3e, 4e) further confirm a North China affinity (Liu et al., 2014a; Xu and Liu, 2020). Thus, felsic melanosomes and leucosomes represented by samples L6, M6, L7, and M7 originated from the Jiaobei terrane.

In contrast to these Paleoproterozoic ages, two zircon grains from mafic melanosome MG1 with low HREE concentrations and low Th/U values yield U-Pb ages of 234–221 Ma (Fig. 5e), while two (likely inherited) zircon cores from granite G0 give U-Pb ages of 719–614 Ma (Fig. 6c). These ages correspond well with the timing of Triassic UHP metamorphism (Fig. 9b) and Neoproterozoic protoliths in the Sulu orogen, which has been proposed as an important source for Jurassic partial melting. Elsewhere within the Jiaodong Peninsula, Jurassic leucosomes have been identified in the Weihai area (Feng et al., 2020; Liu et al., 2010a, 2012), and inherited zircons of Sulu affinity have also been identified in Jurassic granitoids (Huang et al., 2006; Wu et al., 2005; Zhang et al., 2010). Therefore, the mafic migmatites may represent pervasively retrogressed eclogites (Huang et al., 2006) from the Sulu orogen that served as a source for at least some Jurassic granites.

Overall, Paleoproterozoic metamorphic and anatectic zircon (domains) for the protoliths of the felsic migmatites in the Sulu orogen indicate a North China affinity. In contrast, Triassic inherited (metamorphic) zircons from the mafic migmatites (garnet/clinopyroxene amphibolite) indicate a South China affinity. This interpretation implies mixing of protoliths from both the North and South China blocks, which has also been reported in the North Dabie terrane (Xu and Zhang, 2018).

5.2. *Jurassic metamorphic-anatectic event in the Jiaodong Peninsula*

As mentioned above, the Jiaodong Peninsula (including the Jiaobei terrane and Sulu orogen) has a complicated metamorphic and magmatic history. Although the Late Mesozoic granitoids have been ascribed to post-orogenic extension and/or Paleo-Pacific subduction, their petrogenesis and tectonic setting remain ambiguous. Jurassic leucosomes are scattered across the Sulu UHP orogen (Feng et al., 2020, 2021; Liu et al., 2010a, 2012) and could indicate Jurassic partial melting of the Triassic thickened crust during post-orogenic extensional collapse (Feng et al., 2020, 2021; Guo et al., 2005; Zhao et al., 2017b). However, clear temporal or geochemical correspondence between partial melting in parent rocks and the Late Mesozoic magmatism has not yet been documented.

In this study, leucosomes and melanosomes always coexist in the same migmatite outcrops (Fig. 2a, b, e) and are likely genetically related. The melanosomes are residues of partial melts that formed the leucosomes. The thin leucosome veins in the mafic migmatites are also likely products of in-situ melting (Fig. 2e). Many zircon domains have high U, low Th, and low Th/U values, including domains with low CL intensities or weak oscillatory zoning (felsic samples L7 and L6; Figs. 3b, 4b). Inclusions of quartz, K-feldspar, and plagioclase in these zircon domains and steeply positive REE patterns with high HREE contents (Figs. 3f, 4h; Liu et al., 2012) demonstrate that they are all anatectic in origin (e.g., Rubatto et al., 2001). Their U-Pb ages are 155 ± 2 Ma and 160 ± 4 Ma for L7 and L6, respectively (omitting four analyses from L6 with U-Pb ages of 211–186 Ma; Figs. 3e, 4f).

Homogeneous gray zircons from mafic migmatite samples (clinopyroxene amphibolite MG2 and garnet amphibolite MG1) (Fig. 5a, b) also exhibit high U, low Th, and low Th/U values (Table S1), again suggesting a metamorphic origin. Their elevated HREE contents and patterns further indicate that they were formed either without or with a small amount of garnet. These zircons yielded U-Pb ages of 154 ± 2 Ma and 149 ± 4 Ma, respectively (Fig. 5c, e). Similar Jurassic (c. 150 Ma) metamorphic ages occur in titanite from (epidote-bearing) garnet amphibolite in the Rushan area (Fig. 7c). The agreement between titanite and anatectic zircon ages further demonstrates that a

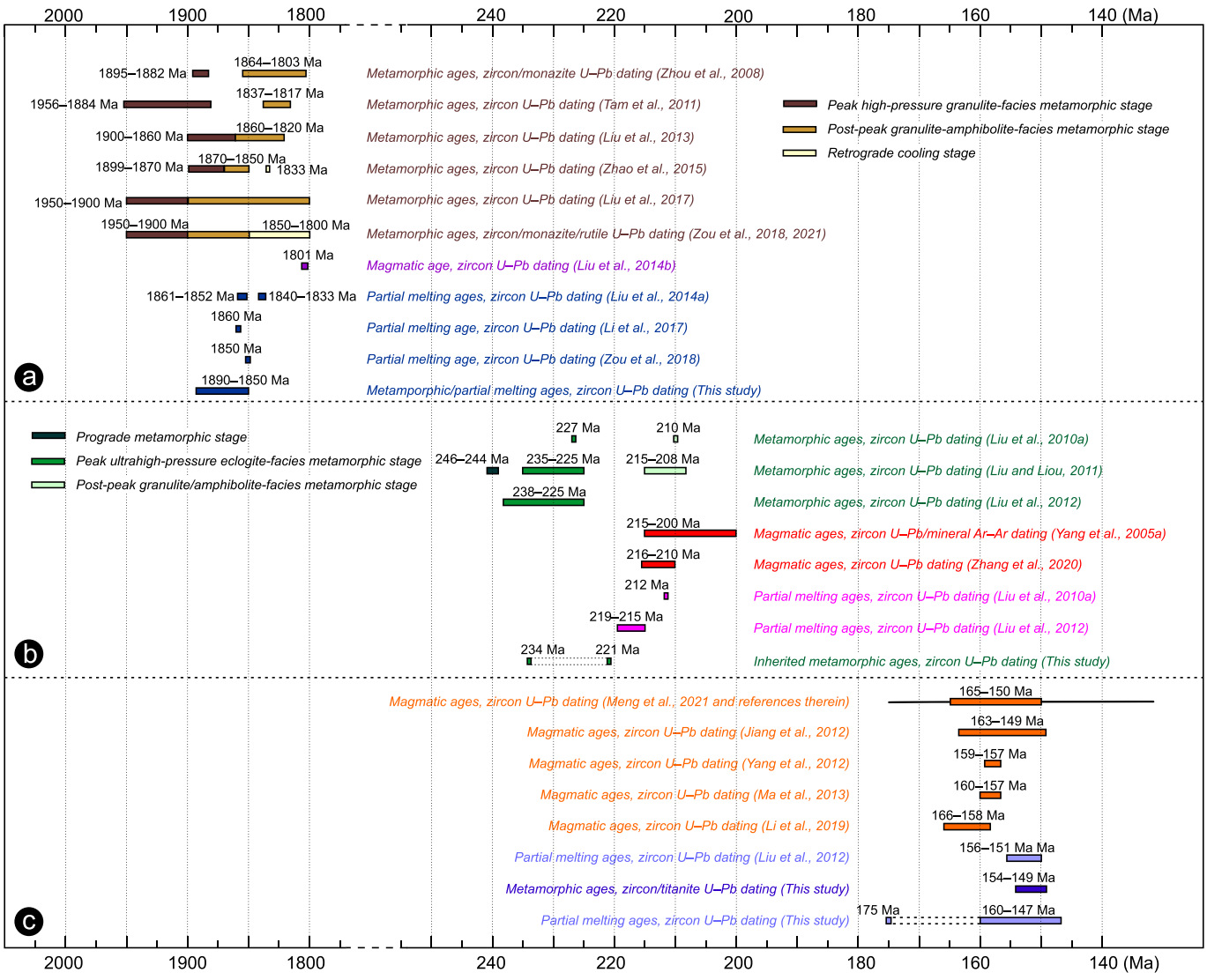

Fig. 9. Summary of metamorphism, magmatism, and partial melting for the Paleoproterozoic in the Jiaobei terrane, the Triassic in the northern Sulu UHP orogen, and the Jurassic in the Jiaodong Peninsula, eastern China.

metamorphic-anatectic event was widespread during the Late Jurassic (c. 155 Ma) in the Rushan-Yantai area of the Jiaodong Peninsula (Fig. 9c). For garnet amphibolite sample MG5, Zr-in-titanite temperatures of 650–750 °C (assuming $P = 8$ kbar) demonstrate that the metamorphic P–T conditions reached amphibolite-facies at c. 150 Ma. For granite sample G1, overgrowth rims on zircons indicate an older anatectic age of 175 Ma, suggesting that the metamorphic-anatectic event started since the Middle Jurassic, prior to intrusion of later abundant Late Jurassic plutons. Thus, we propose a long-lived partial melting scenario for the continental crust in the Jiaodong Peninsula during the Middle to Late Jurassic.

In general, a complete orogenic cycle includes crustal thickening followed by erosional or extensional thinning, while partial melting can take place at almost all the stages (depending on temperature and rock type; Dewey et al., 1993; Vanderhaeghe, 2012; Wang et al., 2014). However, post-collisional partial melting and magmatism connected with crustal extension and thinning are generally more common in orogens worldwide (e.g., Foster et al., 2001; He et al., 2011). In the Jiaodong Peninsula, multiple metamorphic-anatectic events occurred during the late Paleoproterozoic and the Late Triassic (Fig. 9). Paleoproterozoic metamorphism and partial melting are related to the Jiao-Liao-Ji orogen, whereas Triassic metamorphism and partial melting are generally linked to the Sulu orogen, associated with exhumation of thickened or subducted crust (Liu et al., 2010a, 2012, 2014a; Feng et al., 2020). Our data demonstrate that Jurassic metamorphism and partial melting took place 30–50 Myr after Sulu orogenesis, during exhumation of Sulu deeply subducted crust. Such long-lived melts or protracted partial melting has rarely been reported for orogens (e.g., Fornelli et al., 2011; Montero et al., 2004). In this region, they reflect a transition from post-orogenic exhumation to extension during initiation of Paleo-Pacific plate subduction in eastern China.

5.3. Implications for the petrogenesis of Jurassic granitoids

Mesozoic granitoids that are widespread throughout eastern China have been studied both geochronologically and geochemically (Wu et al., 2005; Yang et al., 2005a, 2005b; Wu et al., 2019 and references therein). Among them, Triassic and Cretaceous granitoids have the most definitive genesis and tectonic setting. Triassic plutons are alkaline and composed of potassic to ultrapotassic pyroxene syenite and quartz syenite with associated mafic dikes. They intruded into the UHP rocks of the easternmost Sulu orogen at 215–201 Ma, postdating UHP metamorphism (Yang et al., 2005a; Zhang et al., 2020; Fig. 9). To explain these melts, many researchers invoke initial partial melting of subducted

Yangtze lithospheric mantle during exhumation in a transitional setting from collision to extension (Feng et al., 2021; Liu et al., 2010a, 2012; Xu et al., 2013, 2016; Yang et al., 2005a; Zhao et al., 2017b). In contrast, the Cretaceous granitoids are distributed as voluminous plutons across the Sulu UHP orogen into the Jiaobei terrane (Fig. 1) and consist of norite, monzodiorite, monzonite, monzogranite, granodiorite, diorite, and lamprophyre (Yang et al., 2005b; Zhao et al., 2020). Most of these Cretaceous rocks have distinctively adakitic compositions with high Sr contents, high Sr/Y, and high $\delta^{18}O$ values, generated by partial melting of either thickened lower crust or lithospheric mantle with extensive crust-mantle interaction (Wang et al., 2007; Xu et al., 2007, 2013; Yang et al., 2005b; Zhang et al., 2002). They are not directly related to the Triassic Sulu collision or exhumation but correlate instead to roll-back of the subducted Paleo-Pacific slab, which induced lithospheric thinning during the Early Cretaceous (Yang et al., 2005b).

In contrast to Triassic and Cretaceous plutons, the petrogenesis of Jurassic granitoids is not well understood. Jurassic granitoids are widespread from the Sulu orogen to the Jiaobei terrane, mainly containing the Linglong and Kunyushan plutons (Fig. 1). Their emplacement ages are 180–155 Ma, mostly between 165 and 150 Ma (Meng and Lin, 2021 and references therein; Fig. 9). This age is about 50–80 Myr after the collision between the North and South China blocks and 30–50 Myr after exhumation of deeply subducted crust. Thus, they are unlikely to be related to the Sulu orogenic cycle. Although some researchers have hypothesized that Jurassic magmatism could corelate with Paleo-Pacific plate subduction (Wu et al., 2019 and references therein), Paleo-Pacific plate subduction initiated in the Late Triassic or Early Jurassic (Wu et al., 2019; Zhu et al., 2013), prior to Late Jurassic magmatism. From the perspective of petrogenesis, previous studies suggested that the Jurassic granitoids resulted from partial melting of thickened lower crust with limited crust-mantle interaction triggered by lithospheric thinning and asthenosphere mantle upwelling (Fig. 9; Jiang et al., 2012; Yang et al., 2012; Ma et al., 2013; Zhao et al., 2017a; Li et al., 2019). Zircon Hf model ages and O isotopes, of magmatic zircons from these granitoids together with geochemical data suggest that these rocks originated from both the Archean-Paleoproterozoic basement of the North China block and the Neoproterozoic rocks of the Yangtze block (Wu et al., 2005; Zhang et al., 2010). However, direct evidence of Jurassic metamorphism and partial melting has not yet been identified in the Jiaobei terrane. To date, sparse Jurassic partial melts have been reported only in the Sulu orogen (Feng et al., 2020; Liu et al., 2012).

As mentioned in section 5.2., both metamorphic (154–149 Ma) and anatectic (160–155 Ma) zircon domains are now identified from migmatites in the Jiaodong Peninsula (Figs. 3–5). Moreover, for granite sample G1, anatectic zircon rims with ages of 159–147 Ma overgrew magmatic zircon cores with an age of c. 175 Ma (Fig. 6). This evidence shows that Late Jurassic partial melting took place not only in mafic and felsic metamorphic rocks but also in granitoids. High HREE contents of the anatectic zircon domains (Figs. 3–5) suggest that Jurassic partial melting occurred under garnet-free conditions (e.g., Rubatto, 2002). Higher Th contents and Th/U values (Tables S1–S5) further indicate that the anatectic zircons might have crystallized from hydrous melts. Metamorphic titanite from meta-mafic rocks, as a product of moderate grade metamorphism, yields overlapping Late Jurassic ages (c. 150 Ma) with metamorphic and anatectic zircons. An origin from amphibolite-facies partial melts (migmatites) is consistent with relatively lower zircon saturation temperatures (720–790 °C) for older Jurassic (165–150 Ma) granitoids (Ma et al., 2013; Zhang et al., 2010). If so, the protracted Jurassic metamorphic-anatectic scenario we propose for the continental crust induced contemporaneous and protracted magmatism.

Geochemistry of leucosomes L6 and L7 compared to granite G1 further support an anatectic origin for Jurassic plutons. These leucosomes are exposed adjacent to melanosomes M7 and M6, indicating that they likely represent melts segregated from surrounding parent rocks. Both leucosomes and granite exhibit high Sr/Y values and plot within the adakite region on a Sr/Y vs. Y diagram (Fig. 8c), suggesting they derive from slab (crustal) melting rather than the mantle (Defant and Drummond, 1990). Additionally, the leucosomes have elevated SiO_2 and low MgO contents, falling within the range of experimental melts produced from metabasalt and eclogite at pressures of 1.0–4.0 GPa (Fig. 8a; Rapp et al., 1999). These observations suggest that the granites evolute from leucosomes in response to crustal thickening without significant contribution from mantle components. In a regional geologic context, the Jurassic melts likely resulted from partial melting of the thickened Sulu orogenic roots, which was triggered by/along with a metamorphic event. These partial melts coalesced continuously to form plutons, similar to models for Mesozoic plutonism in the North Dabie Orogen (Xu and Zhang, 2017).

As mentioned above, inherited metamorphic or anatectic zircons from the parent rocks of migmatites clearly indicate that both the Jiaobei terrane and the Sulu orogen were involved in the Late Jurassic metamorphic-anatectic event. Our new observations provide robust evidence for multiple sources (both the North and South China blocks) for the Jurassic granitoids in the Jiaodong Peninsula. The initiation and duration of partial melting match well with the timing of granitic magmatism (Fig. 8; Jiang et al., 2012; Yang et al., 2012; Ma et al., 2013; Li et al., 2019; Meng and Lin, 2021) indicating that some anatectic melts ultimately gathered to form larger magma bodies. These results further constrain the duration and conditions of long-lived partial melts and magmatism, which has been identified in many orogens (e.g., Ding et al., 2021; Ganade de Araujo et al., 2014), as well as in the North Dabie orogen (Xu and Zhang, 2017, 2018). Jurassic anatexis and magmatism play crucial roles in unraveling the source and origin of later Cretaceous magmatism, which has conventionally been ascribed to the collapse of the Triassic orogen. However, additional investigation involving phase equilibrium modeling of Jurassic metamorphism and anatexis are required to accurately establish the connection between migmatites and the associated magmatism. Such research may help promote a comprehensive understanding of the tectonic evolution of the Jiaodong Peninsula throughout the entire Mesozoic era.

6. Conclusions

Petrological, morphological, geochronological, and chemical studies of zircon and titanite from migmatites in the Jiaodong Peninsula provide robust evidence for Jurassic metamorphism and partial melting in both the Jiaobei terrane and the northern Sulu orogen. Key observations and interpretations include:

(1) Metamorphic zircon and titanite and anatectic zircon were identified in migmatites including felsic leucosomes (biotite-plagioclase gneisses), mafic melanosomes (garnet/clinopyroxene amphibolite), and granites in the Yantai-Rushan area; together they record a coincident Late Jurassic (160–147 Ma) metamorphism and partial melting event.
(2) Zircon from melanosomes records Paleoproterozoic metamorphic or magmatic (or anatectic) ages, indicating an affinity with the Jiaobei terrane (North China block); in contrast inherited zircon from leucosomes and garnet amphibolite yields Neoproterozoic magmatic and Triassic metamorphic ages, indicating an affinity with the Sulu orogen (South China block). Thus, both the Jiaobei terrane and Sulu orogen experienced Jurassic metamorphism and partial melting.
(3) Jurassic granitoids in the Jiaodong Peninsula were derived from protracted partial melting of crust from both the North and South China blocks; possibly partial melting extended into the Cretaceous to produce even younger plutons.

Declaration of competing interest

The authors have no conflicts of interest to declare that are relevant to the content of this article.

Acknowledgements

We appreciate constructive comments from Editor-in-Chief Dicheng Zhu, two anonymous reviewers, and Prof. Fulai Liu. Financial support from the National Natural Science Foundation of China (Grants 42002067 and 41890832), the US National Science Foundation (EAR 2118114) and the Beijing Normal University at Zhuhai (310432109, 03700-312223501501) are thanked.

Appendix A. Descriptions of analytical methods

A.1. Zircon cathodoluminescence (CL) and titanite backscatter electron (BSE) imaging

Zircon and titanite grains from crushed rocks were separated using standard density and magnetic techniques, then handpicked under a binocular microscope. The selected crystals were embedded in 25 mm-diameter epoxy disks and polished to approximately half their thickness. We collected zircon CL images using a scanning electron microscope (SEM; JSM 6150.cl) equipped with a Gatan MiniCl detector with a voltage of 10 kV and obtained titanite BSE images using a TESCAN MIRA3 SEM with an accelerating voltage of 20 kV and a working distance of c. 16 mm. These images, combined with transmitted- and reflected-light photomicrographs, were used for revealing zircon and titanite internal structures and for targeting different zones for U-Pb dating.

A.2. U-Pb and trace element analysis of zircon and titanite by laser ablation inductively coupled plasma-mass spectrometry (LA-ICP-MS)

Zircon grains from samples M7, L7, M6, L6, MG1, and G1 and titanite grains from sample MG5 were analyzed by LA-ICP-MS for their U-Pb and trace element compositions. Zircon and titanite analyses were collected at Beijing Createch Testing Technology Co. Ltd. and Beijing Quick-Thermo Science and Technology Co. Ltd., respectively. The devices used to analyze zircon and titanite were an AnlyitikJena PQMS Elite ICP-MS and an Agilent 8900 ICP-QQQ, respectively, both with an ESI NWR 193 nm LA system. The laser beams had diameters of 25–35 μm for zircon and 40 μm for titanite and had a frequency of 10 Hz. Argon was used as the make-up gas and mixed with helium carrier gas via a T-connector before entering the ICP-MS. Each analysis consisted of approximately 15 s of background acquisition and 45 s of data acquisition. Analysis of the glass standard NIST610 and standard minerals followed every set of 5–10 sample analyses (Liu et al., 2010b). Zircon standards include GJ-1, 91,500, and Plešovice, and titanite standards were QLT-1 and Mount Dromedary. The software package ICPMSDataCal was used for data processing. The $^{207}Pb/^{206}Pb$, $^{206}Pb/^{238}U$ and $^{207}Pb/^{235}U$ values were corrected for the error induced by elemental and isotopic fractionation, using 91,500 for zircon and QLT-1 for titanite as external standards. The preferred U–Th–Pb isotopic ratios of 91,500 are from Wiedenbeck et al. (1995), and the uncertainty in the preferred values (0.5%) was propagated to the final data table. Background subtraction and correction for laser downhole elemental fractionation were performed for titanite analysis using the Iolite data reduction package within the Wavemetrics Igor Pro data analysis software (Paton et al., 2010). Variable amounts of titanite common Pb were corrected using a modified version of the VizualAge U-Pb data reduction scheme embedded in Iolite (Chew et al., 2014). The U, Th, Pb, and rare earth element (REE) concentrations of both zircon and titanite were calibrated using NIST 610. Isoplot 4.15 (Ludwig, 2012) was used to create U-Pb concordia plots for zircon and U-Pb Tera-Wasserburg inverse concordia diagrams for titanite; all data for zircon are presented with 1σ errors and 90% confidence limits and those for titanite with 2σ errors.

A.3. Zircon U-Pb analysis by secondary ion mass spectroscopy

U-Pb ages of zircon grains from mafic migmatite sample MG2 were measured on a SHRIMP II instrument at the Beijing SHRIMP Center, Institute of Geology, CAGS. The analytical procedures and conditions were similar to those described by Williams (1998). The analysis spot size was 25 μm, the intensity of the primary O^{2-} ion beam was 3–6 nA, and each spot was rastered for 150–180 s prior to analysis to remove surface contamination. The TEMORA zircon ($^{206}Pb/^{238}U$ age = 417 Ma) was used as a standard to calibrate U abundance and U-Pb age and was analyzed once after every four sample analyses. Analysis at each spot consisted of five scans through a mass sequence that included Zr_2O^+, $^{204}Pb^+$, background, $^{206}Pb^+$, $^{207}Pb^+$, $^{208}Pb^+$, $^{238}U^+$, $^{232}Th^{16}O^+$, and $^{238}U^{16}O^+$ analyzed on a single electron multiplier by cyclic stepping of the magnetic field. Data processing was carried out using the SQUID and ISOPLOT programs. The uncertainties of individual analyses are < 2% at 1σ. The mean weighted ages were calculated at 95% confidence.

Zircon grains from granite sample G0 were analyzed for U-Pb ages using a Cameca IMS 1280HR ion microprobe at the Institute of Geology and Geophysics, Chinese Academy of Sciences (IGGCAS). Li et al. (2009) outlined the analytical procedures. U–Th–Pb abundances and ratios were determined relative to the Plešovice zircon standard (Sláma et al., 2008) with Qinghu zircon (Li et al., 2013) as the monitoring standard. The primary O^{2-} ion beam was focused with a spot size of 20 × 30 μm. A long-term uncertainty of 1.5% (1 RSD, relative standard deviation) for the $^{206}Pb/^{238}U$ measurements of the standard zircons was propagated to the unknowns (Li et al., 2010), although the measured $^{206}Pb/^{238}U$ error in a specific session was ≤1% (1 RSD). A single electron multiplier was used to measure secondary ion beam intensities in peak jumping mode. The Qinghu zircon standard yields consistent ages of 161.7 ± 2.4 Ma to 157.6 ± 2.3 Ma with a concordia age of 160.1 ± 2.0 Ma, within error of the recommended age (159.5 ± 0.2 Ma; Li et al., 2013). The uncertainties of individual analyses are < 2% at 1σ.

A.4. Whole-rock analysis of migmatites and granites

Whole-rock samples of leucosomes L7 and L6 and granite G1 were cut into slabs, and the fresh portions were crushed in a corundum jaw crusher and powdered in an agate mill to < 200 mesh. Major element compositions were measured by X-ray fluorescence (XRF; PW4400) on fused glass beads and trace element compositions was determined by ICP-MS (PE300D), at the National Research Center of Geoanalysis, CAGS. Analytical uncertainties were estimated to be ±3–5% for major oxides and ≤ 5% for most trace elements. The FeO contents were determined by Fe^{2+} titration, and the Fe_2O_3 contents were calculated by difference. National standards of China of GB/T14506.28–2010 and GB/T1456.2–2010 were executed for major and trace element analysis, respectively.

Appendix B. Supplementary data

Supplementary data to this article can be found online at https://doi.org/10.1016/j.lithos.2024.107525.

References

Brown, M., 1994. The generation, segregation, ascent and emplacement of granite magma: the migmatite-to-crustally-derived granite connection in thicked orogens. Earth Sci. Rev. 36 (1), 83–130.
Brown, M., Averkin, Y.A., Mclellan, E., 1995. Melt segregation in migmatites. J. Geophys. Res. 100 (B8), 655–679.
Brown, C.R., Yakymchuk, C., Brown, M., Fanning, C.M., Korhonen, F.J., Piccoli, P.M., Siddoway, C.S., 2016. From source to sink: petrogenesis of cretaceous anatectic granites from the Fosdick migmatite–granite complex, West Antarctica. J. Petrol. 57 (7), 1241–1278.
Chen, Y.X., Zheng, Y.F., Hu, Z.C., 2013. Synexhumation anatexis of ultrahigh-pressure metamorphic rocks: Petrological evidence from granitic gneiss in the Sulu orogen. Lithos 156–159, 69–96.

Chen, R.X., Ding, B., Zheng, Y.F., Hu, Z., 2015. Multiple episodes of anatexis in a collisional orogen: Zircon evidence from migmatite in the Dabie orogen. Lithos 212-215, 247–265.
Cherniak, D.J., Watson, E.B., 2001. Pb diffusion in zircon. Chem. Geol. 172 (1), 5–24.
Chew, D.M., Petrus, J.A., Kamber, B.S., 2014. U–Pb LA–ICPMS dating using accessory mineral standards with variable common Pb. Chem. Geol. 363, 185–199.
Defant, M.J., Drummond, M.S., 1990. Derivation of some modern arc magmas by melting of young subducted lithosphere. Nature 347 (6294), 662–665.
Dewey, J.F., Ryan, P.D., Andersen, T.B., 1993. Orogenic uplift and collapse, crustal thickness, fabrics and metamorphic phase changes: the role of eclogites. Geol. Soc. Lond. Spec. Publ. 76 (1), 325–343.
Ding, H.X., Kohn, M.J., Zhang, Z.M., 2021. Long-lived (ca. 22–24 Myr) partial melts in the eastern Himalaya: Petrochronologic constraints and tectonic implications. Earth Planet. Sci. Lett. 558, 116764.
Faure, M., Lin, W., Monié, P., Le Breton, N., Poussineau, S., Panis, D., Deloule, E., 2003. Exhumation tectonics of the ultrahigh–pressure metamorphic rocks in the Qinling orogen in East China: New petrological-structural-radiometric insights from the Shandong Peninsula. Tectonics 22, 1018.
Feng, P., Wang, L., Brown, M., Wang, S., Li, X., 2020. Separating multiple episodes of partial melting in polyorogenic crust: an example from the Haiyangsuo complex, northern Sulu belt, eastern China. GSA Bull. 132 (5–6), 1235–1256.
Feng, P., Wang, L., Brown, M., Johnson, T.E., Kylander-Clark, A., Piccoli, P.M., 2021. Partial melting of ultrahigh-pressure eclogite by omphacite-breakdown facilitates exhumation of deeply-subducted crust. Earth Planet. Sci. Lett. 554, 116664.
Fornelli, A., Langone, A., Micheletti, F., Piccarreta, G., 2011. Time and duration of Variscan high-temperature metamorphic processes in the south European Variscides: constraints from U-Pb chronology and trace element chemistry of zircon. Mineral. Petrol. 103, 101–122.
Foster, D.A., Schafer, C., Fanning, C.M., Hyndman, D.W., 2001. Relationships between crustal partial melting, plutonism, orogeny, and exhumation: Idaho–Bitterroot batholith. Tectonophysics 342 (3), 313–350.
Ganade de Araujo, C.E., Rubatto, D., Hermann, J., Cordani, U.G., Caby, R., Basei, M.A.S., 2014. Ediacaran 2500-km-long synchronous deep continental subduction in the West Gondwana Orogen. Nat. Commun. 5 (1), 5198.
Gao, M.D., Xu, H.J., Foley, S.F., Zhang, J.F., Wang, Y., 2023. Ultrahigh pressure mantle metasomatism in continental collision zones recorded by post-collisional mafic rocks. GSA Bull. 135 (11–12), 3066–3082.
Guo, J.H., Chen, F.K., Zhang, X.M., Siebel, W., Zhai, M.G., 2005. Evolution of syn-to post-collisional magmatism from north Sulu UHP belt, eastern China:zircon U–Pb geochronology. Acta Petrol. Sin. 21, 1281–1301 (in Chinese).
Hacker, B.R., Wallis, S.R., Ratschbacher, L., Grove, M., Gehrels, B., 2006. High-temperature geochronology constraints on the tectonic history and architecture of the ultrahigh-pressure Dabie-Sulu Orogen. Tectonics 25 (TC5006).
Hayden, L.A., Watson, E.B., Wark, D.A., 2008. A thermobarometer for sphene (titanite). Contrib. Mineral. Petrol. 155 (4), 529–540.
He, Y.S., Li, S.G., Hoefs, J.C., Huang, F., Liu, S.A., Hou, Z.H., 2011. Post-collisional granitoids from the Dabie orogen: New evidence for partial melting of a thickened continental crust. Geochim. Cosmochim. Acta 75, 3815–3838.
Huang, J., Zheng, Y.F., Zhao, Z.F., Wu, Y.B., Zhou, J.B., Liu, X.M., 2006. Melting of subducted continent: element and isotopic evidence for a genetic relationship between Neoproterozoic and Mesozoic granitoids in the Sulu orogen. Chem. Geol. 229 (4), 227–256.
Jiang, N., Chen, J.Z., Guo, J.H., Chang, G.H., 2012. In situ zircon U–Pb, oxygen and hafnium isotopic compositions of Jurassic granites from the North China Craton: Evidence for Triassic subduction of continental crust and subsequent metamorphism-related ^{18}O depletion. Lithos 142–143, 84–94.
Kohn, M.J., 2017. Titanite petrochronology. Rev. Mineral. Geochem. 83, 419–441.
Labrousse, L., Prouteau, G., Ganzhorn, A.C., 2011. Continental exhumation triggered by partial melting at ultrahigh pressure. Geology 39 (12), 1171–1174.
Li, X.H., Liu, Y., Li, Q.L., Guo, C.H., Chamberlain, K.R., 2009. Precise determination of Phanerozoic zircon Pb/Pb age by multicollector SIMS without external standardization. Geochem. Geophys. Geosyst. 10 (4), Q04010.
Li, X.H., Long, W.G., Li, Q.L., Liu, Y., Zheng, Y.F., Yang, Y.H., Chamberlain, K.R., Wan, D. F., Guo, C.H., Wang, X.C., Tao, H., 2010. Penglai zircon megacrysts: A potential new working reference material for microbeam determination of Hf–O isotopes and U–Pb age. Geostand. Geoanal. Res. 34 (2), 117–134.
Li, X.H., Tang, G.Q., Gong, B., Yang, Y.H., Hou, K.J., Hu, Z.C., Li, Q.L., Liu, Y., Li, W.X., 2013. Qinghu zircon: a working reference for microbeam analysis of U-Pb age and Hf and O isotopes. Chin. Sci. Bull. 58, 4647–4654.
Li, Y.L., Zhang, H.F., Guo, J.H., Li, C.F., 2017. Petrogenesis of the Huili paleoproterozoic leucogranite in the Jiaobei Terrane of the North China Craton: a highly fractionated albite granite forced by K-feldspar fractionation. Chem. Geol. 450, 165–182.
Li, X.H., Fan, H.R., Hu, F.F., Hollings, P., Yang, K.F., Liu, X., 2019. Linking lithospheric thinning and magmatic evolution of late Jurassic to early cretaceous granitoids in the Jiaobei Terrane, southeastern North China Craton. Lithos 324–325, 280–296.
Liu, F.L., Liou, J.G., 2011. Zircon as the best mineral for P–T–time history of UHP metamorphism: A review on mineral inclusions and U–Pb SHRIMP ages of zircons from the Dabie–Sulu UHP rocks. J. Asian Earth Sci. 40 (1), 1–39.
Liu, F.L., Robinson, P.T., Gerdes, A., Xue, H.M., Liu, P.H., Liou, J.G., 2010a. Zircon U–Pb ages, REE concentrations and Hf isotope compositions of granitic leucosome and pegmatite from the north Sulu UHP terrane in China: constraints on the timing and nature of partial melting. Lithos 117 (1), 247–268.
Liu, Y.S., Gao, S., Hu, Z.C., Gao, C.G., Zong, K.Q., Wang, D.B., 2010b. Continental and oceanic crust recycling-induced melt–peridotite interactions in the Trans-North China Orogen: U–Pb Dating, Hf isotopes and trace elements in zircons from mantle xenoliths. J. Petrol. 51 (1–2), 392–399.
Liu, F.L., Robinson, P.T., Liu, P.H., 2012. Multiple partial melting events in the Sulu UHP terrane: zircon U–Pb dating of granitic leucosomes within amphibolite and gneiss. J. Metamorph. Geol. 30 (8), 887–906.
Liu, P.H., Liu, F.L., Liu, C.H., Wang, F., Liu, J.H., Yang, H., Cai, J., Shi, J.R., 2013. Petrogenesis, *P–T–t* path, and tectonic significance of high-pressure mafic granulites from the Jiaobei terrane, North China Craton. Precambrian Res. 233, 237–258.
Liu, F.L., Liu, P.H., Wang, F., Liu, J.H., Meng, E., Cai, J., Shi, J.R., 2014a. U–Pb dating of zircons from granitic leucosomes in migmatites of the Jiaobei Terrane, southwestern Jiao–Liao–Ji Belt, North China Craton: Constraints on the timing and nature of partial melting. Precambrian Res. 245, 80–99.
Liu, J.H., Liu, F.L., Ding, Z.J., Liu, P.H., Guo, C.L., Wang, F., 2014b. Geochronology, petrogenesis and tectonic implications of Paleoproterozoic granitoid rocks in the Jiaobei Terrane, North China Craton. Precambrian Res. 255, 685–698.
Liu, P.H., Liu, F.L., Cai, J., Wang, F., Liu, C.H., Liu, J.H., Yang, H., Shi, J.R., Liu, L.S., 2017. Discovery and geological significance of high-pressure mafic granulites in the Pingdu–Anqiu area of the Jiaobei Terrane, the Jiao–Liao–Ji Belt, the North China Craton. Precambrian Res. 303, 445–469.
Liu, F.L., Liu, L.S., Cai, J., Liu, P.H., Wang, F., Liu, C.H., Liu, J.H., 2019. A widespread Paleoproterozoic partial melting event within the Jiao-Liao-Ji Belt, North China Craton: Zircon U-Pb dating of granitic leucosomes within pelitic granulites and its tectonic implications. Precambrian Res. 326, 155–173.
Ludwig, K., 2012. Isoplot 4.15: a geochronological toolkit for Microsoft Excel. In: Berkeley Geochronology Center Special Publication (Version 4.15) Berkeley Geochronology Center.
Ma, L., Jiang, S.Y., Dai, B.Z., Jiang, Y.H., Hou, M.L., Pu, W., Xu, B., 2013. Multiple sources for the origin of Late Jurassic Linglong adakitic granite in the Shandong Peninsula, eastern China: zircon U–Pb geochronological, geochemical and Sr–Nd–Hf isotopic evidence. Lithos 162–163, 251–263.
Meng, L.T., Lin, W., 2021. Episodic crustal extension and contraction characterizing the late mesozoic tectonics of East China: evidence from the Jiaodong Peninsula, East China. Tectonics 40 (3) (e2020TC006318).
Montero, P., Bea, F., Zinger, T.F., Scarrow, J.H., Molina, J.F., Whitehouse, M.J., 2004. 55 million years of continuous anatexis in Central Iberia: single zircon dating of the Pena Negra complex. J. Geol. Soc. Lond. 161, 1–11.
Paton, C., Woodhead, J.D., Hellstrom, J.C., Hergt, J.M., Greig, A., Maas, R., 2010. Improved laser ablation U-Pb zircon geochronology through robust downhole fractionation correction. Geochem. Geophys. Geosyst. 11, Q0AA06.
Rapp, R.P., Shimizu, N., Norman, M.D., Applegate, G.S., 1999. Reaction between slab-derived melts and peridotite in the mantle wedge: experimental constraints at 3.8 GPa. Chem. Geol. 160 (4), 335–356.
Rubatto, D., 2002. Zircon trace element geochemistry: partitioning with garnet and the link between U–Pb ages and metamorphism. Chem. Geol. 184 (1), 123–138.
Rubatto, D., Williams, I.S., Buick, I.S., 2001. Zircon and monazite response to prograde metamorphism in the Reynolds Range, Central Australia. Contrib. Mineral. Petrol. 140 (4), 458–468.
Sláma, J., Košler, J., Condon, D.J., Crowley, J.L., Gerdes, A., Hanchar, J.M., Horstwood, M.S.A., Morris, G.A., Nasdala, L., Norberg, N., Schaltegger, U., Schoene, B., Tubrett, M.N., Whitehouse, M.J., 2008. Plešovice zircon—a new natural reference material for U–Pb and Hf isotopic microanalysis. Chem. Geol. 249 (1–2), 1–35.
Tam, P.Y., Zhao, G.C., Liu, F.L., Zhou, X.W., Sun, M., Li, S.Z., 2011. Timing of metamorphism in the Paleoproterozoic Jiao-Liao-Ji Belt: new SHRIMP U–Pb zircon dating of granulites, gneisses and marbles of the Jiaobei massif in the North China Craton. Gondwana Res. 19 (1), 150–162.
Vanderhaeghe, O., 2012. The thermal–mechanical evolution of crustal orogenic belts at convergent plate boundaries: a reappraisal of the orogenic cycle. J. Geodyn. 56–57, 124–145.
Wang, Q., Wyman, D.A., Xu, J.F., Jian, P., Zhao, Z.H., Li, C.F., Xu, W., Ma, J.L., He, B., 2007. Early cretaceous adakitic granites in the Northern Dabie complex, Central China: Implications for partial melting and delamination of thickened lower crust. Geochim. Cosmochim. Acta 71 (10), 2609–2636.
Wang, L., Kusky, T.M., Polat, A., Wang, S.J., Jiang, X.F., Zong, K.Q., Wang, J.P., Deng, H., Fu, J.M., 2014. Partial melting of deeply subducted eclogite from the Sulu orogen in China. Nat. Commun. 5 (1), 5604.
Wiedenbeck, M., Alle, P., Corfu, F., Griffin, W.L., Meier, M., Oberli, F., von Quadt, A., Roddick, J.C., Spiegel, W., 1995. Three natural zricon standards for U-Th-Pb, Lu-Hf, trace element and REE analyses. Geostand. Newslett. 19 (1), 1–23.
Williams, I.S., 1998. U-Th-Pb geochronology by ion microprobe. In: McKibben, M.A., Shanks, W.C., Ridley, W.I. (Eds.), Applications of Microanalytical Techniques to Understanding Mineralizing Processes. Review of Economic Geology, 7, pp. 1–35.
Wu, F.Y., Lin, J.Q., Wilde, S.A., Zhang, X.O., Yang, J.H., 2005. Nature and significance of the early cretaceous giant igneous event in eastern China. Earth Planet. Sci. Lett. 233 (1), 103–119.
Wu, F.Y., Yang, J.H., Xu, Y.G., Wilde, S.A., Walker, R.J., 2019. Destruction of the North China craton in the mesozoic. Annu. Rev. Earth Planet. Sci. 47, 173–195.
Wu, H.J., He, Y.S., Li, S.G., Zhu, C.W., Hou, Z.H., 2020. Partial melts of intermediate-felsic sources in a wedged thickened crust: insights from granites in the Sulu orogen. J. Petrol. 61 (5) (egaa053).
Xu, W., Liu, F.L., 2020. Geochronological and geochemical insights into the tectonic evolution of the Paleoproterozoic Jiao-Liao-Ji Belt, Sino-Korean Craton. Earth Sci. Rev. 193, 162–198.
Xu, H.J., Zhang, J.F., 2017. Anatexis witnessed post-collisional evolution of the Dabie orogen, China. J. Asian Earth Sci. 145, 278–296.
Xu, H.J., Zhang, J.F., 2018. Zircon geochronological evidence for participation of the North China Craton in the protolith of migmatite of the North Dabie Terrane. J. Earth Sci. 29 (1), 30–42.

Xu, J.F., Shinjo, R., Defant, M.J., Wang, Q., Rapp, R.P., 2002. Origin of Mesozoic adakitic intrusive rocks in the Ningzhen area of East China: Partial melting of delaminated lower continental crust? Geology 30 (12), 1111.
Xu, H.J., Ma, C.Q., Ye, K., 2007. Early cretaceous granitoids and their implications for the collapse of the Dabie orogen, eastern China: SHRIMP zircon U–Pb dating and geochemistry. Chem. Geol. 240 (3), 238–259.
Xu, H.J., Ye, K., Song, Y.R., Chen, Y., Zhang, J.F., Liu, Q., Guo, S., 2013. Prograde metamorphism, decompressional partial melting and subsequent melt fractional crystallization in the Weihai migmatitic gneisses, Sulu UHP terrane, eastern China. Chem. Geol. 341, 16–37.
Xu, H.J., Zhang, J.F., Wang, Y.F., Liu, W.L., 2016. Late Triassic alkaline complex in the Sulu UHP terrane: Implications for post-collisional magmatism and subsequent fractional crystallization. Gondwana Res. 35, 390–410.
Yakymchuk, C., Kirkland, C.L., Clark, C., 2018. Th/U ratios in metamorphism zircon. J. Metamorph. Geol. 36 (6), 715–737.
Yang, J.H., Chung, S.L., Wilde, S.A., Wu, F.Y., Chu, M.F., Lo, C.H., Fan, H.R., 2005a. Petrogenesis of post-orogenic syenites in the Sulu Orogenic Belt, East China: geochronological, geochemical and Nd–Sr isotopic evidence. Chem. Geol. 214 (1–2), 99–125.
Yang, J.H., Wu, F.Y., Chung, S.L., Wilde, S.A., Chu, M.F., Lo, C.H., Song, B., 2005b. Petrogenesis of early cretaceous intrusions in the Sulu ultrahigh-pressure orogenic belt, East China and their relationship to lithospheric thinning. Chem. Geol. 222 (3), 200–231.
Yang, K.F., Fan, H.R., Santosh, M., Hu, F.F., Wilde, S.A., Lan, T.G., Lu, L.N., Liu, Y.S., 2012. Reactivation of the Archean lower crust: implications for zircon geochronology, elemental and Sr–Nd–Hf isotopic geochemistry of late Mesozoic granitoids from northwestern Jiaodong Terrane, the North China Craton. Lithos 146, 112–127.
Zhang, H.F., Gao, S., Zhong, Z.Q., Zhang, B.R., Zhang, L., Hu, S.H., 2002. Geochemical and Sr–Nd–Pb isotopic compositions of cretaceous granitoids: constraints on tectonic framework and crustal structure of the Dabieshan ultrahigh-pressure metamorphic belt, China. Chem. Geol. 186 (3), 281–299.
Zhang, J., Zhao, Z.F., Zheng, Y.F., Dai, M.N., 2010. Postcollisional magmatism: geochemical constraints on the petrogenesis of Mesozoic granitoids in the Sulu orogen, China. Lithos 119 (3), 512–536.
Zhang, H.Y., Blenkinsop, T., Yu, Z.W., 2020. Timing of Triassic tectonic division and postcollisional extension in the eastern part of the Jiaodong Peninsula. Gondwana Res. 83, 141–156.
Zhao, L., Li, T.S., Peng, P., Guo, J.H., Wang, W., Wang, H.Z., Santosh, M., Zhai, M.G., 2015. Anatomy of zircon growth in high pressure granulites: SIMS U–Pb geochronology and Lu–Hf isotopes from the Jiaobei Terrane, eastern North China Craton. Gondwana Res. 28 (4), 1372–1390.
Zhao, Z.F., Liu, Z.B., Chen, Q., 2017a. Melting of subducted continental crust: Geochemical evidence from Mesozoic granitoids in the Dabie-Sulu orogenic belt, east-Central China. J. Asian Earth Sci. 145, 260–277.
Zhao, Z.F., Zheng, Y.F., Chen, Y.X., Sun, G.C., 2017b. Partial melting of subducted continental crust: Geochemical evidence from synexhumation granite in the Sulu orogen. GSA Bull. 129 (11–12), 1692–1707.
Zhao, Z.X., Liang, S.N., Santosh, M., Wei, J.H., 2020. Lithospheric extension associated with slab rollback: Insights from early cretaceous magmatism in the southern segment of Tan-Lu fault zone, Central-Eastern China. Lithos 362–363, 105487.
Zhou, X.W., Zhao, G.C., Wei, C.J., Geng, Y.S., Sun, M., 2008. EPMA U–Th–Pb monazite and SHRIMP U–Pb zircon geochronology of high-pressure pelitic granulites in the Jiaobei massif of the north China Craton. Am. J. Sci. 308 (3), 328–350.
Zhou, K., Chen, Y.X., Zheng, Y.F., Xu, L.J., 2019. Migmatites record multiple episodes of crustal anatexis and geochemical differentiation in the Sulu ultrahigh-pressure metamorphic zone, eastern China. J. Metamorph. Geol. 37 (8), 1099–1127.
Zhu, K.Y., Li, Z.X., Xu, X.S., Wilde, S.A., 2013. Late Triassic melting of a thickened crust in southeastern China: evidence for flat-slab subduction of the Paleo-Pacific plate. J. Asian Earth Sci. 74, 265–279.
Zou, Y., Zhai, M.G., Santosh, M., Zhou, L.G., Zhao, L., Lu, J.S., Liu, B., Shan, H.X., 2018. Contrasting P–T–t paths from a Paleoproterozoic metamorphic orogen: Petrology, phase equilibria, zircon and monazite geochronology of metapelites from the Jiao-Liao-Ji belt, North China Craton. Precambrian Res. 311, 74–97.
Zou, Y., Li, Q.L., Chu, X., Zhai, M.G., Mitchell, R.N., Zhao, L., Zhou, L.G., Wang, Y.Q., Liu, B., 2021. Older orogens cooled slower: new constraints on Orosirian tectonics from garnet diffusion modeling of metamorphic timescales, Jiaobei terrain, North China Craton. Contrib. Mineral. Petrol. 176 (11), 91.